Phthalocyanines—Versatile Components of Molecular Conductors

Tamotsu Inabe*

Division of Chemistry, Graduate School of Science, Hokkaido University, Sapporo 060-0810, Japan

Hiroyuki Tajima*

Institute for Solid State Physics, University of Tokyo, Kashiwanoha, Kashiwa, Chiba 277-8581, Japan

Received March 17, 2004

Contents

* To whom correspondence should be addressed. T.I.: Phone: +81-11-706-3511. Fax: +81-11-706-3511. E-mail: inabe@sci.hokudai.ac.jp. H.T.: Phone: +81-471-36-3235. Fax: +81-471-36-3236. E-mail: tajima@issp.u-tokyo.ac.jp.

1. Introduction

Phthalocyanine is a very stable π-conjugated macrocyclic ligand that can form metal complexes with almost all the metal elements. Also, in most of cases, the planarity of the ligand is retained. The molecules are well known as dyes due to their chemical and thermal stability and very strong characteristic optical absorption in the visible region, the so-called Q-band. The molecules can also be utilized for photoconductor, photomemory, solar cell, electrochromic display, deodorizer, sensor, etc., and many studies on the application or development of functionalities have been pursued.[1] The physical properties of the assembly are varied by the structure of the ligand, relative molecular arrangement, and central metal. Therefore, various functionalities can be produced by controlling such parameters.

Electrical conductivity can usually be realized by making the π-ligand open shell after oxidizing the ligand. A rich variety of conductors have been developed by changing the degree of oxidation, molecular arrangement, and chemical species of the central metal.

In this review, we focus on the molecular materials of which structures have been determined. It is well known that there are various axial ligand bridging polymers. Most of them are conducting when they are appropriately doped, but some are conducting without dopant. Such polymers are described in the other reviews.[2–4]

In this review, the sections are classified mainly by the chemical structure. The porphyrinic systems are also included as analogues of the phthalocyanine systems, Chart 1.

10.1021/cr030649x CCC: $48.50
Published on Web 09/16/2004

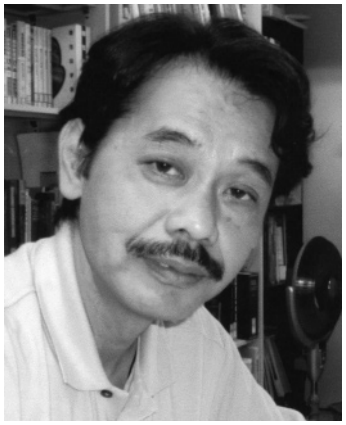

Tamotsu Inabe was born in 1954 in Hokkaido, Japan. He received his B.Sc. degree in 1976 and Ph.D. degree in 1981 from Hokkaido University under the supervision of Professor Y. Matsunaga in the field of solid-state chemistry of molecular materials. Then he joined the solid-state group of Professor T. J. Marks at Northwestern University as a postdoctoral fellow . His research focused on phthalocyanine conductors. In 1984 he was appointed as a research associate at the Institute for Molecular Science (IMS). He was promoted to Associate Professor of the Department of Chemistry, Faculty of Science, Hokkaido University, in 1992 and became Full Professor in 1993. He has been studying structures and properties of molecular crystals. The target materials are phthalocyanines, organic charge-transfer complexes, hydrogen-bonding molecular crystals, crystals with magnetic moments, etc. New materials design is the most important subject of his research.

Hiroyuki Tajima was born in 1958 in Tokyo, Japan. He received his B.S. degree in 1981 from the University of Tokyo with a major in Chemistry. He obtained his M.S. degree at the Department of Chemistry, Faculty of Science, University of Tokyo, in 1983 under the supervision of Professor Haruo Kuroda. In 1986 he obtained his Ph.D. degree in the same department with a thesis on optical study for conducting molecular crystals. From 1986 to 1988 he performed postdoctoral research at Research Development Corporation of Japan (ERATO project), where he studied fabrication techniques of thin films. In 1988 he returned to the Department of Chemistry, University of Tokyo, as an Assistant Professor. He was promoted to Lecturer in 1993 in the same department, and he then moved to the Institute of Solid State Physics, University of Tokyo, as an Associate Professor in 1996. His main research techniques are optical and magneto-transport measurements. His current interests are electronic properties on molecular assemblies such as molecular conductors and molecular thin-film devices.

1.1. Partially Oxidized Salt

When the Pc unit is planar M(Pc) (M = H_2 for the metal-free compound), the compounds are represented by M(Pc)X_y. In this formula X is a monovalent anion and y takes a fractional value between 0 and 1. Depending on M or applying pressure, the oxidized part becomes not only the Pc π system but also the central metal. Historically, compounds with X = I_3^- were the oldest, and the compounds are described first followed by the salts with other closed-shell anions. Then, in section 3, the porphyrinic systems are described. These partially oxidized salts are composed of one-dimensional columns of planar macrocyclic π-conjugated ligand complexes, while recently, the Pc conductors composed of axially substituted partially oxidized units, $[M^{III}(Pc)Z_2]^{\rho-}$, have been developed. In these crystals the Pc units form not only one-dimensional stacks but also higher dimensional stacking structures, owing to the steric effect of the axial substituents. These partially oxidized salt crystals are described in section 4.

Chart 1

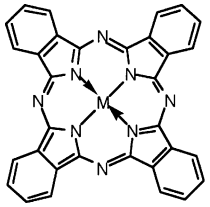

M(phthalocyaninato) (M(Pc))

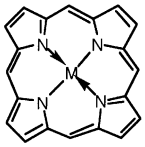

M(porphyrinato)

1.2. Neutral Radical Crystals

Since the closed-shell Pc ligand is a divalent anion, complexes with divalent metals are neutral and in general insulators. There are three cases where complexes are neutral but composed of the mono-anion radical ligand and metals, as follows.

(1) Complexes composed of a monovalent metal and a monoanionic Pc radical (Li(Pc)).

(2) Sandwich-type complexes composed of a trivalent metal and a closed-shell dianionic and an open-shell monoanionic Pc ligand.

(3) Complexes composed of an open-shell monoanionic Pc ligand and a trivalent metal and two anionic axial ligands or a divalent metal and an anionic axial ligand.

They are not a metallic conductor, but some show high conductivity. These crystals are described in section 5.

2. Face-to-face Stacked Partially Oxidized M(Pc)X_y Systems

2.1. Ni(Pc) Salts

Commercially obtained Ni(Pc) is not very pure, and multiple sublimation in a vacuum has been applied for purification. However, this method is not very effective in removing M′(Pc) (M′ is the other transition metal). Very pure Ni(Pc) was obtained from direct metalation of pure H_2(Pc).[5] The sample purity was found to seriously affect the physical properties as shown below.

The highest occupied d orbital in the Ni(Pc) is $3d_{z^2}$. The energy level of this orbital is comparable to that of the highest occupied π orbital (π-HOMO) having a_{1u} symmetry. Charge-transfer (CT) complexes are formed by oxidation of Ni(Pc). In these complexes under ambient pressure only the π-HOMO is oxi-

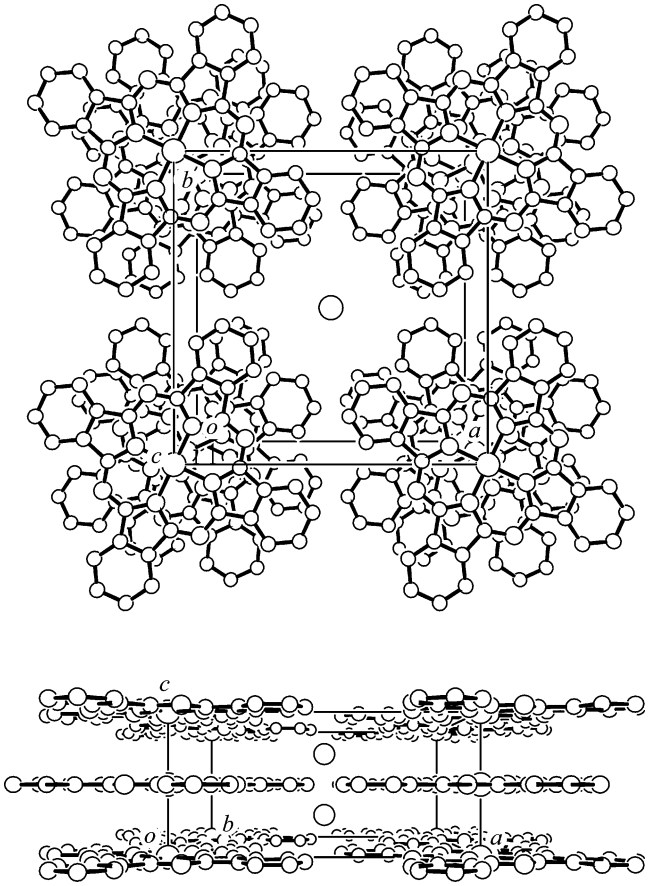

Figure 1. Crystal structure of Ni(Pc)I.

dized, and the d_{z^2} orbital is not oxidized. According to Yakushi, however, 3 d_{z^2} is also oxidized under applied pressure.[6]

2.1.1 Ni(Pc)I

The first report on Pc conductors was published in 1977,[7] in which highly conducting black powder was obtained when M(Pc) (M = Fe, Co, Ni, Cu, Zn, Pt, H_2) was oxidized with iodine. After this report the single-crystal structure and physical properties were studied in detail on the compound with M = Ni.[8] The single crystals were grown by a slow diffusion method in which Ni(Pc) and iodine were put in each leg of the H-tube adding 1-chloronaphthalene as the solvent, and the Ni(Pc) side was heated at about 100 °C. Single crystals of the other iodinated Pc salts were obtained by a similar method.

The crystal system is tetragonal with a space group *P4/mcc*. Ni(Pc) is planar and stacks along the *c* axis, forming a one-dimensional (1D) column, as shown in Figure 1. The neighboring Ni(Pc) molecules in the column are not eclipsed but rotating by about 40°. Iodine atoms align in the channel formed between the Ni(Pc) columns, forming a chain with equally separated atoms. Each atom locates at the special position but has elongated temperature factors along the chain. This structure is interpreted as an averaged picture of the I_3^- chains without interchain correlations (Figure 2). The assignment of the anion species as I_3^- has been confirmed by Raman and ^{129}I Mössbauer spectra.[8] Therefore, though the chemical composition is represented by Ni(Pc)I, the real electronic state is $[Ni(Pc)]^{+0.33}(I_3^-)_{0.33}$. This situation is in agreement with the other M(Pc)'s. The crystal data of the $M(Pc)X_y$-type crystals are summarized in Table 1.

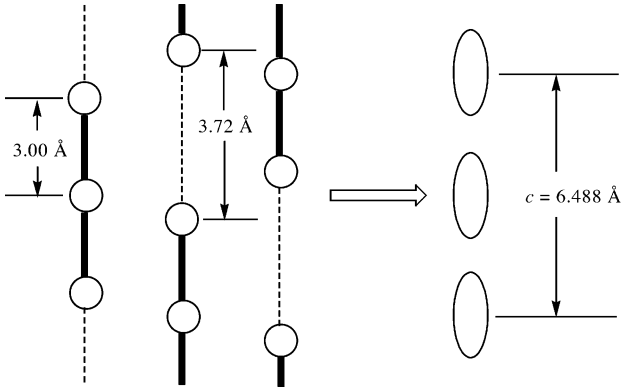

Figure 2. Disorder model for the iodine chains in Ni(Pc)I.

In this crystal, starting neutral $Ni^{II}(Pc^{2-})$ becomes a cation with a formal charge of +0.33. Whether the oxidation is metal-centered or π-ligand-centered has been judged by ESR measurements.[8] The *g* value was found to be 2.0007−2.0075, which is a typical value for a π-radical, and there is no possibility of Ni^{III}. Therefore, in this crystal one electron is removed from every three Pc ligands and the HOMO of the Pc π system forms a 5/6-filled metallic 1D band. The bandwidth was estimated from magnetic susceptibility, reflectance spectra, and thermoelectric power measurements.

The paramagnetic susceptibility is temperature-independent and can be considered as Pauli-like paramagnetism. By assuming a 1D tight-binding band model, bandwidth was estimated to be $4t = 0.37$ eV.[8, 5] This value is somewhat lower compared with those estimated from other methods (vide infra), which is interpreted as enhancement of the susceptibility due to the on-site Coulomb repulsion.

The reflectance spectra show typical behavior of a 1D conductor; with the light polarized parallel to the Pc 1D column, the spectrum shows a clear plasma edge beginning at 4500 cm^{-1}, while there is no dispersion with the light perpendicular to it.[9] By using the observed plasma frequency and assuming the 1D tight-binding band structure, the bandwidth was estimated to be 0.84 eV, which is larger than that estimated from the susceptibility measurements.

The thermoelectric power (TEP) along the Pc column shows metallic behavior; the TEP linearly correlates with temperature above 100 K.[9] Again, by assuming the 1D tight-binding band structure, the bandwidth was estimated to be 0.88 eV, which is in good agreement with that estimated from the reflectance spectra.

The above three physical properties clearly indicate that this crystal has metallic properties along the Pc stacking direction. There was a historical process until the intrinsic electrical conductivity of the single-crystal became clear. In the first paper in 1980[8] the room-temperature conductivity along the *c* axis was reported to be 550 S cm^{-1} and a metal-like temperature dependence was observed. However, the conductivity showed a sudden drop at 55 K (Figure 5a).

Table 1. Space Group, Cell Parameters, and Interplanar Spacing of M(Pc)X_y-type and M(Pc)$_2I_x$-type Conductors

compound	space group	cell parameters/Å	cell volume/Å^3	Z	temp/K	interplanar spacing/Å	ref
Ni(Pc)I	*P*4/*mcc*	a = 13.936(6) c = 6.488(3)	1260	2		3.244	8
Ni(Pc)Br	*P*4/*mcc*	a = 13.793(7) c = 6.431(4)	1224	2	167	3.216	12
Ni(Pc)$(BF_4)_{0.33}$	*P*4/*mcc*	a = 13.97(2) c = 6.48(1)	1265	2	300	3.240	13
Ni(Pc)$(ClO_4)_{0.42}$	*P*4/*mcc*	a = 13.957(3) c = 6.467(1)	1260	2	296	3.233	14
	*P*4/*mnc*	a = 19.543(8) c = 6.416(4)	2450	4	153	3.208	14
$[Ni(Pc)]_2(SbF_6)$	*Pnc*2	a = 14.113(1) b = 28.710(2) c = 6.441(2)	2610	2		3.221	15
$[Ni(Pc)]_2(AsF_6)$	*Pnc*2	a = 14.015(1) b = 28.485(2) c = 6.466(3)	2581	2		3.233	16
H_2(Pc)I	*P*4/*mcc*	a = 13.979(6) c = 6.502(3)	1271	2	298	3.251	8
Cu(Pc)I	*P*4/*mcc*	a = 13.888(12) c = 6.390(8)	1232	2	114	3.195	30
Co(Pc)I	*P*4/*mcc*	a = 13.927(1) c = 6.247(1)	1212	2	116	3.123	38
Co(Pc)$(AsF_6)_{0.5}$	*P*4/*mcc*	a = 14.234(2) c = 6.296(2)	1276	2		3.148	41
Pt(Pc)$(ClO_4)_{0.5}$	*P*4/*mcc*	a = 14.062(1) c = 6.510(1)	1287	2	r.t.	3.255	45
Fe(Pc)I	*P*4/*mcc*	a = 13.84(2) c = 6.77(1)	1320	2	97	3.38	47
Bi$(Pc)_2I_{3/2}$	*P*4/*mcc*	a = 13.997(2) c = 6.549(1)	1283	1		3.275	48
Yb$(Pc)_2I_2$	*P*4/*mcc*	a = 13.927(2) c = 6.409(1)	1243	1	295	3.205	49
As$(Pc)_2I_2$	*P*4/*mcc*	a = 13.926(2) c = 6.433(1)	1248	1	295	3.217	49
In$(Pc)_2I_2$	*P*4/*mcc*	a = 13.984(2) c = 6.393(1)	1250	1		3.197	50
Ti$(Pc)_2I_2$	*P*4/*mcc*	a = 13.841(3) c = 6.370(3)	1220	1	113	nonplanar	51
U$(Pc)_2I_{5/3}$	*P*4/*mcc*	a = 13.947(2) c = 6.501(1)	1265	1		3.251	52
U$(Pc)_2I_2$	*P*4/*nnc*	a = 19.731(2) c = 6.507(1)	2533	2		3.253	53
Zr$(Pc)_2I_2$	*P*4/*mcc*	a = 13.941(2) c = 6.487(1)	1261	1		3.244	50

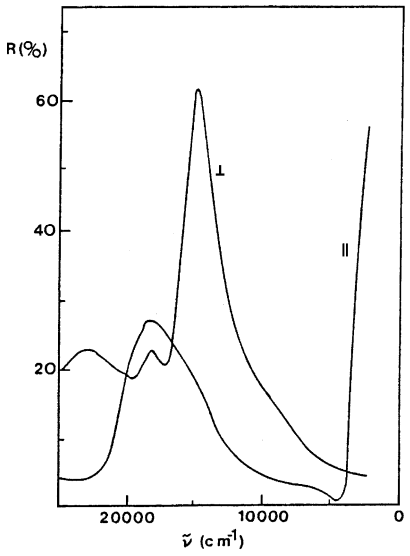

Figure 3. Polarized reflectance spectra of Ni(Pc)I. The parallel (∥) orientation has the electric field polarized along the highly conducting stacking axis, while the perpendicular (⊥) orientation has the electric field polarized perpendicular to the stacking axis. (Reprinted with permission from ref 9. Copyright 1984 American Physical Society.)

This discontinuous conductivity change was not reproducible and speculated as extrinsic, such as microcracks due to the mechanical stress on the crystal by the temperature change. At that time, however, it was thought that some transition to an insulating state should occur, since the electronic structure is a typical 1D system. Two reports on the temperature dependence with neither irreversibility nor discontinuity appeared in 1983. In one of them[10]

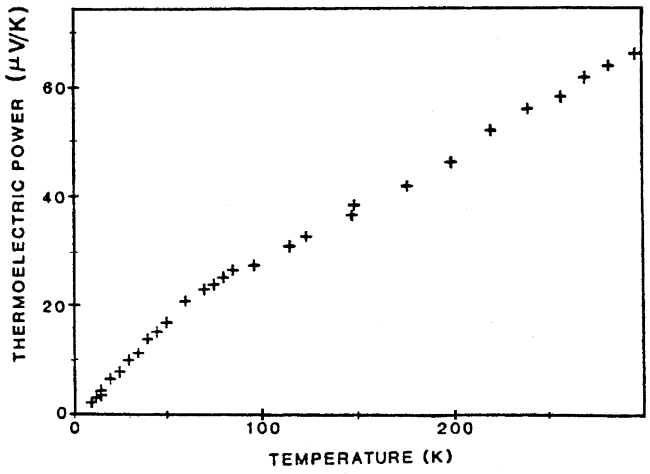

Figure 4. Temperature dependence of the thermoelectric power of Ni(Pc)I. (Reprinted with permission from ref 9. Copyright 1984 American Physical Society.)

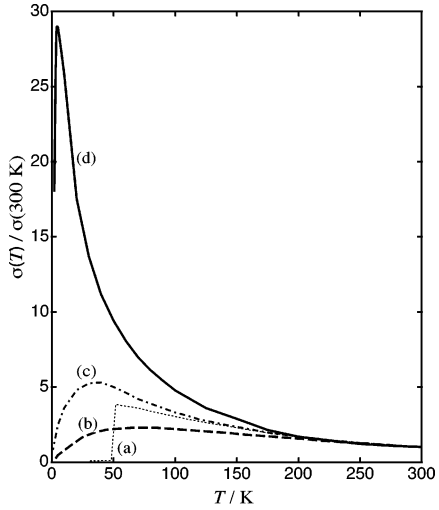

Figure 5. Temperature dependence of the conductivities of Ni(Pc)I. The conductivity data are replotted: (a) ref 8, (b) ref 10, (c) ref 9, and (d) ref 5 (the purest sample).

the conductivity showed a broad maximum around 80 K and decreased gradually with lowering temperature (Figure 5b). In the other paper[9] the conductivity continuously increased down to 25 K and showed a broad maximum at that temperature (Figure 5c). The conductivity at the lowest temperature (100 mK) was as high as that at room temperature. At that time it was not clear why this discrepancy occurred, though in the latter paper special care was taken to eliminate the stress on the sample crystal. It was speculated that some extrinsic origin might operate, since no clear anomaly was observed in the other physical properties where the maximum conductivity was observed.[9]

This speculation was proved by the paper in 1993.[5] In this paper, extreme care was paid to preparation of the starting Ni(Pc), and the paramagnetic impurity level was decreased as low as 170 ppm. The conductivity of the resultant Ni(Pc)I continuously increased down to 5 K and only slightly decreased below that temperature (Figure 5d). The maximum conductivity reached a value 30 times higher than the room-temperature conductivity. When the sample purity was lowered, a decrease of the maximum conductivity and an increase of the temperature where the maximum conductivity occurred were observed, in accord with the impurity level. Preparation of the high-purity sample was rather difficult, since it was found that conventional vacuum sublimation could not remove the paramagnetic impurity completely.

From the above results it became clear that Ni(Pc)I maintains metallic properties at very low temperature. It is rather curious since the electronic structure is a typical 1D system that should suffer intrinsic instabilities. This point was interpreted as follows. The one-dimensionality in Ni(Pc)I is considerably strong compared with the other 1D systems, and the intercolumnar interaction is extremely weak. In addition, there is a disordered tri-iodide lattice. These factors may suppress the three-dimensional ordering process for the insulating ground state.

The pressure dependence of the conductivity of Ni(Pc)I was reported for the high-purity sample.[11]

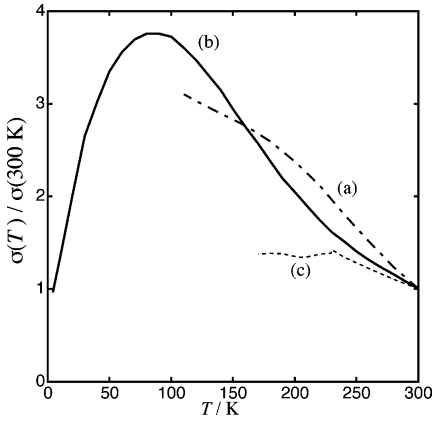

Figure 6. Temperature dependence of the electrical conductivities of (a) Ni(Pc)Br [ref 12], (b) $Ni(Pc)(BF_4)_{0.33}$ [ref 13], and (c) $Ni(Pc)(ClO_4)_{0.42}$ [ref 14]. The conductivity data are replotted.

Under relatively low pressure (~3 kbar), a metal-to-insulator transition was observed at 30 K. This transition became blurred at higher pressures, and the metallic phase again stabilized at low temperature.

2.1.1. Ni(Pc)Br

As an analogous system to Ni(Pc)I, Ni(Pc)Br was studied.[12] Crystal growth was performed by a method similar to that of Ni(Pc)I but with 1,2,4-trichlorobenzene as a solvent. The crystal structure is isomorphous with Ni(Pc)I, and the *a* axis length is shortened due to the smaller halogen size (13.793 Å in Ni(Pc)Br vs 13.936 Å in Ni(Pc)I). The Br atoms were found at the positions of iodine in Ni(Pc)I and analyzed as a disordered Br_3^- chain. Though Br_3^- is appreciably shorter than I_3^-, the one-third of the oxidation state of the Pc ligand is so stable that the Br_3^- anions fall into the same *c* axis length. Electrical conductivity was measured only above 100 K due to its fragile mechanical property (Figure 6a). The conductivity at room temperature was 150 S cm^{-1}, and its metallic behavior was much weaker than that of Ni(Pc)I. The line width of the ESR spectra increased below 100 K, which is in contrast to the constant value of Ni(Pc)I.

2.1.2. $Ni(Pc)(BF_4)_{0.33}$

This partially oxidized salt is the first Pc conductor obtained by electrocrystallization.[13] Since ordinary metal Pc complexes represented by Ni(Pc) are poorly soluble in common solvents for electrochemistry such as acetone, acetonitrile, chloroform, etc., there was no attempt to grow crystals by the electrochemical method. However, this study indicated that electrolysis at high temperature (~100 °C) with a constant current (0.5 μA) in 1-chloronaphthalene solution is effective to grow single crystals on the anode surfaces. After this report many other partially oxidized Pc salts were prepared by electrolysis.

The structure of the obtained crystal was found to be isomorphous with Ni(Pc)I, but accurate atomic parameters were not determined. Since the size of BF_4^- is considerably smaller than that of I_3^-, it is rather curious that BF_4^- is packed in the channel

between the Pc columns to maintain the same oxidation number in both $Ni(Pc)(BF_4)_{0.33}$ and Ni(Pc)I. The conductivity at room temperature was 1000 S cm^{-1} and showed metallic behavior down to 80 K. Below this temperature the conductivity gradually decreased, but even at 1.5 K it is comparable to the room-temperature value (Figure 6b). Since this crystal showed high conductivity at low temperature, the maximum conductivity temperature could shift to the lower temperature for the high-purity sample as observed in Ni(Pc)I. The bandwidth was estimated from the thermoelectric power, reflectance spectra, and magnetic susceptibility measurements and was 1.3, 1.2, and 0.64 eV, respectively.

2.1.3. $Ni(Pc)(ClO_4)_{0.42}$

The partially oxidized salt with ClO_4^- has an unusual composition of $Ni(Pc)(ClO_4)_{0.42}$.[14] The room-temperature structure is isomorphous with Ni(Pc)I, but the site occupation of ClO_4 is 0.42. The crystal undergoes a clear structural transition at 230 K, which is rather rare as the Pc molecular conductor. At this temperature the space group changed from *P4/mcc* to *P4/mnc* and the lattice volume became twice as large. The orientationally disordered ClO_4 at room temperature showed orientational ordering at this transition. However, there was no indication of the superlattice structure along the Pc column direction. Indeed, the thermoelectric power revealed no anomaly at this transition temperature and showed smooth metallic behavior. On the other hand, conductivity measurements were not successful below this temperature (Figure 6c). This was speculated to be due to domain wall phenomena accompanied by the transition rather than microcracks of the crystal. The conductivity at room temperature was 700 S cm^{-1} and showed clear metallic behavior above 230 K. The bandwidth was estimated to be 1.5 eV from both thermoelectric power and reflectance spectra measurements. The slope of the temperature dependence of TEP and the plasma frequency were distinctively different from those observed for Ni(Pc)-$X_{0.33}$.

2.1.4. $[Ni(Pc)]_2(AsF_6)$ and $[Ni(Pc)]_2(SbF_6)$

Finely powdered Ni(Pc) was refluxed in pyridine solution and filtered to remove Co(Pc). This procedure was repeated over 10 times, and then the filtrated Ni(Pc) powder was sublimed in a vacuum several times. Single crystals of $[Ni(Pc)]_2XF_6$ (X = As or Sb) were prepared by electrochemically oxdizing Ni(Pc) in the 1-chloronaphthalene solution at 120 ± 2 °C under Ar atmosphere, n-Bu_4NXF_6 being used as the supporting electrolyte.[15,16] These crystals belong to the orthorhombic system (Table 1). Figure 7 shows the crystal structure of $[Ni(Pc)]_2(SbF_6)$. Contrary to the tetragonal form of the Pc salts, disorder in the anion site does not exist in these crystals. As can be seen from the figure, the overlap of the Ni atom is incomplete and the Ni−Ni chain elongating along the *c* axis is a little bit zigzag-shaped.[15,16]

The electrical conductivity at room temperature is 70−700 S cm^{-1} for the AsF_6 salt and 10−200 S cm^{-1} for the SbF_6 salts.[16,17] The microwave (9.4 GHz)

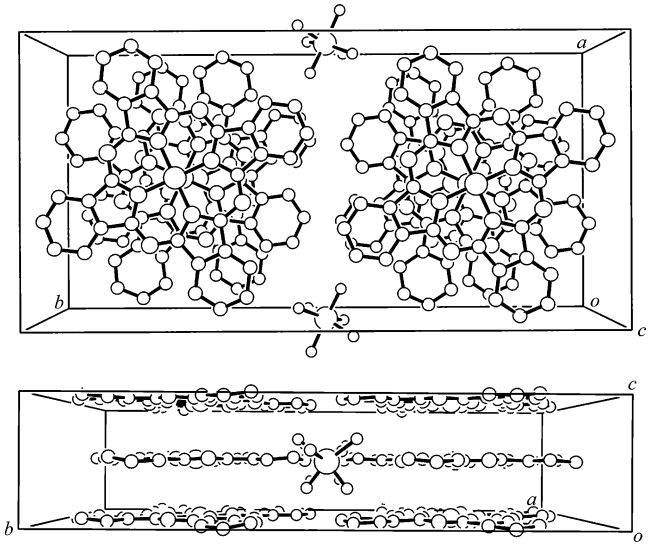

Figure 7. Crystal structure of $Ni(Pc)(SbF_6)_{0.5}$.

conductivity of the AsF_6 salt increased on lowering the temperature to 20 K and decreased below 20 K.[18,19] According to the reflectivity measurements the width of the energy band was estimated to be $4t$ = 1.1 and 1.2 eV for the AsF_6 and SbF_6 salts, respectively.[16] The ESR spectra of AsF_6 crystals are classified into several groups as shown in Figure 8, while

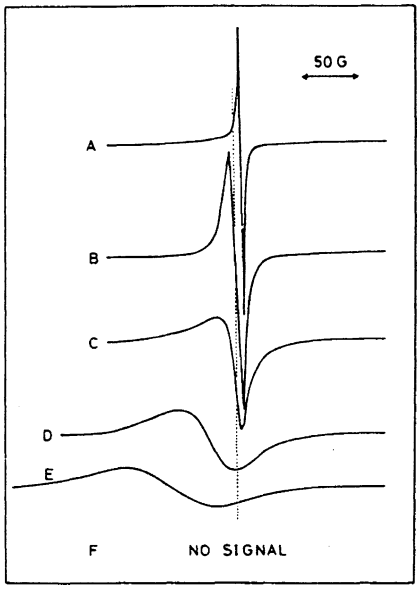

Figure 8. Line shape of the ESR signal of typical crystals of $Ni(Pc)(AsF_6)_{0.5}$. The variance of the spectral line shape can be explained by taking the different concentration of impurity ($Ni^{III}(Pc)$) into consideration (see text). (Reprinted with permission from ref 16. Copyright 1989 Chemical Society of Japan.)

the ESR spectra of the SbF_6 crystals are similar to each other.[16] Except group A of AsF_6 salt, the g tensor of the AsF_6 and SbF_6 salts drastically increased on lowering the temperature. For example, the g value ($H \perp c$) of the SbF_6 salt was 2.031 around room temperature and almost reached to 2.292 (the $g_\perp$ value of $Ni^{III}(Pc)$) around 20 K. To explain the temperature dependence of the $g_\perp$ value and the sample dependence of the ESR spectra, Yakushi et al. proposed a model that the conduction electrons

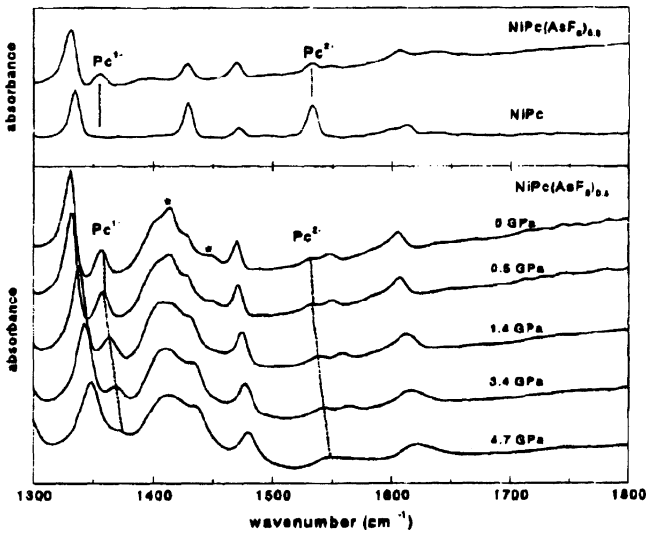

Figure 9. Infrared absorption spectra of $[Ni(Pc)]_2(AsF_6)$. (top) Difference in the phonon structure between the oxidized and unoxidized Ni(Pc). (bottom) Pressure dependence of $[Ni(Pc)]_2(AsF_6)$ in the same spectral region. The asterisks denote absorption by the pressure medium. (Reprinted with permission from ref 6. Copyright 2001 John Wiley & Sons, Ltd.)

are located mainly on the Pc rings and that they exchange rapidly with a localized d electron originating from $Ni^{III}(Pc)$ included in a crystal as a defect. They assumed $\sim 4 \times 10^{-3}$ spin/Ni site and $0-4 \times 10^{-3}$ spin/Ni site included in the SbF_6 and AsF_6 salts, respectively, and explained the temperature dependence of the ESR spectra as well as sample dependence of the ESR spectra for the AsF_6 salt.[16] On the basis of this interpretation, they concluded that AsF_6 and SbF_6 salts are quite similar to each other, the number of defects is smallest in group A of AsF_6 salt, and magnetic susceptibility for the π-conduction band increases on lowering the temperature below 20 K.[16]

The inclusion of a small amount of $Ni^{III}(Pc)$ indicates that the energy levels of d_{z^2} and the π conduction band are very close to each other. Then Yakushi et al. considered $Ni^{III}(Pc)$ might be stabilized under applied pressure. To examine whether such a new electronic state is realized under applied pressure, they did various experiments under applied pressures. The first experiment was a reflectivity measurement for the AsF_6 salt under applied pressures ($P < 1.6$ GPa) using a diamond anvil cell.[20] They found a downward shift of the plasma edge with an increase of pressure. They established that the molecular-vibration band at 1353 cm^{-1} as well as an electronic transition around 18 500 cm^{-1} is a good probe for elucidating the oxidation state of the Pc ring.[21,22] The change of the vibration band reflects the charge redistribution in a Pc ring when the central metal atom is oxidized.[24] Figure 9 shows infrared absorption spectra under applied pressures. As can be seen from the spectra, the 1353 cm^{-1} vibration band decreases its intensity with an increase of pressure and disappears at a pressure of 4.7 GPa. This indicates that the Pc ring is reduced under applied pressure. In other words, the injected hole carriers shift from the Pc ring to the Ni atom. A similar conclusion is obtained from the disappearance

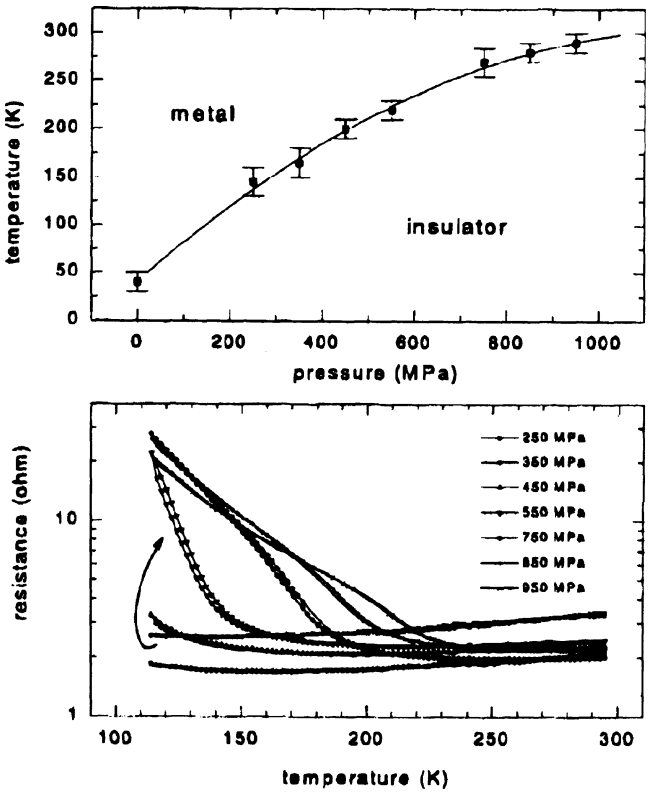

Figure 10. Temperature dependence of the resistance of $[Ni(Pc)]_2(AsF_6)$ at various pressures (bottom), and temperature−pressure phase diagram determined from the resistance measurements (top). (Reprinted with permission from ref 6. Copyright 2001 John Wiley & Sons, Ltd.)

of the electronic transition around 18 500 cm^{-1}.[6] They also deduced that a metal−insulator transition occurred above 5 kbar from the decrease of the plasmon absorption band and concluded that the AsF_6 salts fell into an insulating state as a result of hole transfer from the Pc ring to the Ni atom.[6,19,23] Later this conclusion was verified by resistivity and thermoelectric power measurements under applied pressure.[6,25,26] They determined the temperature−pressure phase diagram (Figure 10) of $[Ni(Pc)]_2(AsF_6)$ from the resistivity measurements under applied pressure. On the basis of the X-ray study under applied pressure, they proposed a model that shortening of the Ni−Ni distance pushed up the $3d_{z^2}$ orbital energy under applied pressure.[6,25,26]

2.2. $H_2(Pc)I$

Observation of the highly conducting properties of this crystal confirmed that charge transport in many Pc materials was due to the π-ligand. The crystal structure is completely isomorphous with Ni(Pc)I, and the difference in the interplanar spacing is also small (3.251 Å in $H_2(Pc)I$ vs 3.244 Å in Ni(Pc)I). The conductivity in the first paper[27] was 700 S cm^{-1} at room temperature and increased to 15 K. Below this temperature the conductivity gradually decreased; however, the value at 1.5 K was still high (5 times the room-temperature value). For this crystal high-purity sample was examined (free-radical impurity < 60 ppm) and the improved data reported.[5] The conductivity at room temperature was 500 S cm^{-1}, the maximum conductivity temperature was 3 K, and

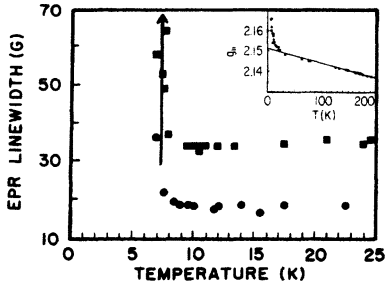

Figure 11. EPR line widths of Cu(Pc)I near the transition temperature. (■: $H_0//c$; ●:$H_0 \perp c$). (inset) Temperature dependence of the g value for $H_0//c$. The temperature dependence above 20 K is explained by eq 2-3-1. (Reprinted with permission from ref 31. Copyright 1986 American Physical Society.)

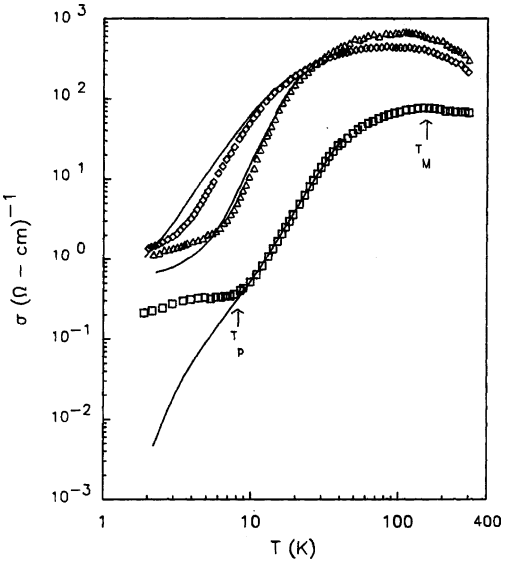

Figure 12. Microwave conductivity (16.8 GHz) as a function of temperature for Cu(Pc)I (□), Cu(tabp)I (△), and Cu(tbp)I (◇) at $H = 0$ T. The solid line shows the data at $H = 8$ T. (Reprinted with permission from ref 33. Copyright 1992 EDP Sciences.)

the maximum value was 31 times the room-temperature value (the data can be seen in Figure 14). The maximum value was maintained even at 1.9 K. The behavior is rather similar to that of pure Ni(Pc)I. For this crystal, when the sample purity was lowered, a decrease of the maximum conductivity and an increase of the maximum conductivity temperature were observed depending on the impurity level.

The magnetic susceptibility and reflectance spectra of H_2(Pc)I were almost identical to those of Ni(Pc)I, and the estimated bandwidth was 0.38 eV from the Pauli-like susceptibility and 1.3 eV from the plasma frequency.

For the high-purity sample, the magnetoresistance measurements were performed.[28] Though below 2 K a relatively steep conductivity decrease was observed, the high conductivity was still maintained at 20 mK (18 times the room-temperature value). The behavior of the magnetoresistance was changed at 2 K, and the sign of the magnetoresistance changed from plus to minus at 1.5 K. This change of the behavior was suggested to be a dimensional crossover from 1D to 3D.

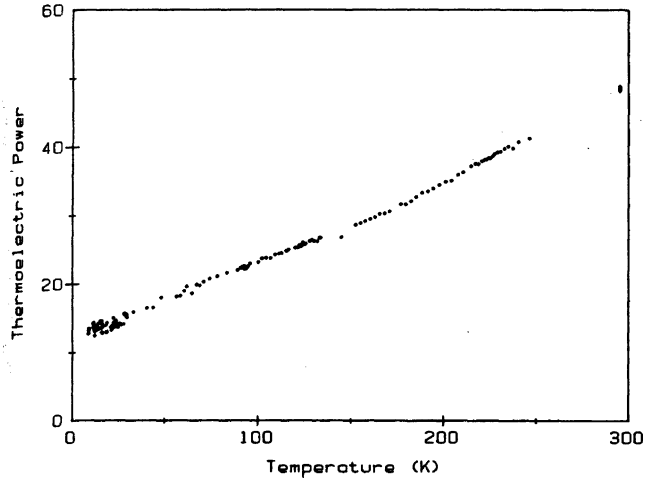

Figure 13. Temperature dependence of the thermoelectric power of Cu(Pc)I. Thermoelectric power decreases almost linearly versus temperature. (Reprinted with permission from ref 30. Copyright 1984 American Chemical Society.)

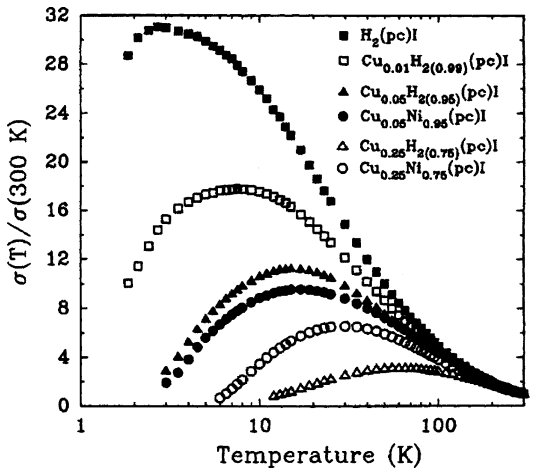

Figure 14. Temperature dependence of the normalized conductivity of $Cu_xH_{2(1-x)}$(Pc)I, $x = 0$, 0.01, 0.05, 0.25, and Cu_xNi_{1-x}(Pc)I, $x = 0.05$ and 0.25. (Reprinted with permission from ref 36. Copyright 1999 American Physical Society.)

2.3. Cu(Pc)I

The highest occupied d orbital in Cu(Pc) is $3d_{x^2-y^2}$, which is a singly occupied orbital. Charge-transfer (CT) complexes are formed by oxidation of Cu(Pc). In this oxidation the π-HOMO is oxidized but the $d_{x^2-y^2}$ orbital is not. Contrary to the $3d_{z^2}$ orbital extending along a stacking axis, the $3d_{x^2-y^2}$orbital is localized in charge-transfer salts of Cu(Pc) and an unpaired electron in this orbital acts as a source of a localized magnetic moment.[29] Therefore, the interplay between the conduction electrons and local magnetic moments is expected in conducting salts of Cu(Pc).

To date, Cu(Pc)I is the only conducting salt of Cu(Pc). The magnetic susceptibility of this salt is expressed by $\chi(T) = \chi_{Cu}(T) + \chi_\pi = C/(T - \Theta) + \chi_\pi$. By assuming $\chi_\pi = 3.8 \times 10^{-4}$emu·mol^{-1} deduced from the susceptibility of Ni(Pc)I, $C = 0.401$ emu·K·mol^{-1}, $\Theta = -4.18$ K was obtained. The evaluated Curie constant C is consistent with the free-spin value $C = N\mu_B^2 g^2 S(S + 1)/3k_B$ with $S = 1/2$. This indicates that an unpaired electron on the $d_{x^2-y^2}$ orbital acts as a local magnetic moment.[30,31]

Due to the rapid exchange between the localized d electrons and conduction electrons, the EPR spectra exhibited a single peak. The temperature dependence of the EPR g value above 20 K is expressed by

$$g_{\parallel obs}(T) = f_{Cu}(T)g_{Cu\parallel} + (1 - f_{Cu}(T))g_{\pi} \quad (2\text{-}3\text{-}1)$$

$$f_{Cu}(T) = \chi_{Cu}(T)/(\chi_{Cu}(T) + \chi_{\pi})$$

Below 20 K, the EPR g value of the coupled system increased anomalously, and at 8 K the EPR signal broadened abruptly and became unobservable (see Figure 11). This phenomenon is reminiscent of a transition into an anitiferromagnetic state. However, the temperature dependence of the magnetic susceptibility as well as proton NMR did not indicate any sign of such transition. To date, development of a static spin-density wave along a stacking axis of amplitude greater than $2 \times 10^{-2}\ \mu_B$ is precluded for this transition.[31]

The dc four-probe conductivity of this salt is about 1000 S cm^{-1} at room temperature. The dc conductivity increased on lowering the temperature, took a maximum at temperatures below 100 K, and then decreased.[30] A similar temperature dependence was also observed in the microwave conductivity above 8 K. Below 8 K, however, significant discrepancy was observed between dc and microwave conductivities.[32] The microwave conductivity versus temperature curve exhibited a plateau below 8 K, while this plateau was missing in the curve of the dc conductivity. When a magnetic field was applied at temperatures lower than 8 K, the plateau for the microwave conductivity disappeared. Similar behavior was also observed in Cu(tatbp)I and Cu(tbp)I. (ref 33: see Figure 12 and section 3.3). The decrease of the microwave conductivity by the magnetic field is significant (σ(8T)/σ(0T) < 0.1 at 2 K). Similar significant change by the magnetic field was also observed in the microwave dielectric constant.[33] According to ref 30, the thermoelectric power (TEP) of this salt almost linearly decreased on lowering the temperature (see Figure 13). However, the TEP value extrapolated to 0 K was 10−15 μV/K, which contrasts with the value expected for metals. According to ref 33, the TEP versus T curve exhibited an inflection around 100 K but the TEP value extrapolated to 0 K was 10−15 μV/K, also in this experiment.

Spectroscopic studies in the visible−ultraviolet region were reported in ref 34, and those in the near-infrared−visible region were reported in ref 30. In the former report, assignment of out-of-plane LMCT and MLCT associated with the d orbital of the central metal were investigated in detail by comparing optical spectra of H_2(Pc)I with that of Cu(Pc)I, Co(Pc)I, and Ni(Pc)I. In the latter report, plasma edge was observed around 4000 cm^{-1} in the reflectance spectrum polarized along the 1D axis. By applying the Drude model to the spectrum, the plasma frequency and bandwidth were, respectively, estimated to be ω_p = 6670 cm^{-1} and $4t$ = 1.45 eV.

The crystal structure of Cu(Pc)I is very similar to that of Ni(Pc)I and H_2(Pc)I, so that they form alloys such as Cu_xM_{1-x}(Pc)I [M = Ni, H_2]. For these alloys EPR (X-band and Q-band), magnetotransport, and magnetic susceptibility were investigated in detail.[32,35−37] According to ref 36, the low-temperature charge-transport properties are seriously affected by the purity of H_2(Pc) and Ni(Pc) for samples with small x. Measurements of magnetic susceptibility for the alloy revealed a linear dependence of the Weiss temperature (Θ) on x.[36] From this dependence Martin and Philips estimated a value for carrier-mediated exchange interaction $J_{e-d} \approx 240$ K.[37] Figure 14 shows a plot of relative dc conductivity ($\sigma_{rel}(T) = \sigma(T)/\sigma$(300K)) versus temperature. All the curves exhibit a peak on lowering the temperature.[36] The peak value (σ_{rel}^{max}) and the temperature at the peak (T_{max}) are functions of x. With an increase of x, σ_{rel}^{max} decreases and T_{max} increases. Both changes are drastic for x < 0.25.

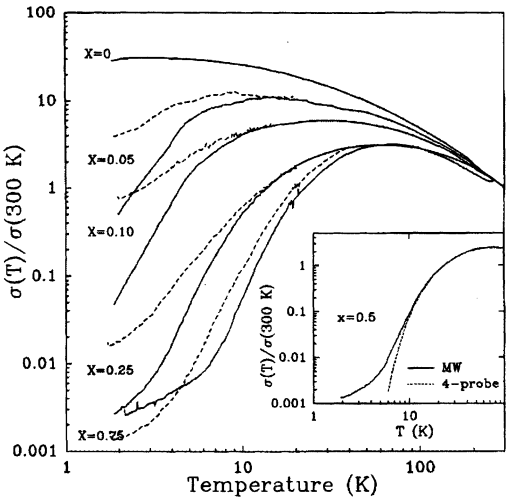

Figure 15. Temperature dependence of the normalized microwave conductivity as a function of temperature for $Cu_xH_{2(1-x)}$(Pc)I with x = 0, 0.05, 0.10, 0.25, 0.75 (dotted line, H = 8 T; solid line, H = 0 T). (inset) Temperature dependence of the normarized dc (dotted line) and microwave (solid line) conductivity for $Cu_{0.5}H_{2(0.5)}$(Pc)I. (Reprinted with permission from ref 36. Copyright 1999 American Physical Society.)

Figure 15 shows the temperature dependence of the microwave conductivity.[36] Although the temperature dependence of the microwave conductivity was very similar to that of dc conductivity in the higher temperature region, serious discrepancy was observed below $T = T_p$ < 10 K. In this temperature range the microwave conductivity exhibited a plateau. This plateau was associated with a magnetic transition observed in the ESR experiments. With a decrease of x, T_p went down and was not observed for x < 0.25. Similar to Cu(Pc)I, the microwave conductivity changes under applied magnetic field. By applying the magnetic field the microwave conductivity tends to increase ($T_{max} > T > T_p$) or decrease ($T_p > T$). In the case of Cu(Pc)I, the former tendency is not obvious. In the alloys, however, both tendencies are obvious. Therefore, the alloys exhibit a very complicated field dependence of the magnetoconductivity, especially at low temperatures.

2.4. Co(Pc) Salts

Co(Pc) has an unpaired electron on the d_{z^2} orbital extending along the 1D axis. In the face-to-face

stacking structure the d_{z^2} orbital of the Co(Pc) molecule overlaps with d_{z^2} orbitals of the next Co(Pc) molecules. Therefore, the unpaired electron couples with other unpaired electrons through the antiferromagnetic exchange interaction and no longer behaves as a free spin. Physical properties of the conducting Co(Pc) salt are different from those of the M(Pc) salts with M ≠ Co. Martinsen et al. ascribed the distinct properties of Co(Pc)I to the difference of the channel into which the charge carriers are injected; Co(Pc)I has a metal-oxidized channel, whereas M(Pc)I (M ≠ Co) have ligand-oxidized channels.[38] However, ligand oxidation was later reported for $[Co(Pc)]_2AsF_6$ by Yakushi et al.[6] At the present stage, whether metal oxidation or ligand oxidation occurs seems to be an unsettled problem in the Co(Pc) salts.

2.4.1. Co(Pc)I

Co(Pc)I has a crystal structure similar to that of Cu(Pc)I and Ni(Pc)I. On the basis of resonant Raman scattering experiments, iodine was found to be in the form of I_3^-. Thus, the explicit formula of this crystal is $[Co(Pc)]^{1/3+}(I_3^-)_{1/3}$. The plasma edge was observed around 6000 cm^{-1} in the reflectance spectrum for the light polarized along the *c* axis (1D axis).[38] This edge is higher than that of either Cu(Pc)I[30] or Ni(Pc)I[9] (~4500 cm^{-1}). The reflectance spectrum exhibits a shoulder around $3-5 \times 10^3$ cm^{-1}, indicating that Co(Pc)I has a narrow band gap.[38] The thermoelectric power of Co(Pc)I is negative, while that of M(Pc)I with M ≠ Co is positive. From the sign of the thermoelectric power, Martinsen et al. proposed a model that the Co d_{z^2} orbital is oxidized instead of the Pc π orbital and the resulting Co d_{z^2} band is one-thirds filled.[38] The magnetic susceptibility of this salt is almost temperature independent, except a Curie tail below 20 K.[38] ESR spectra are also silent except a signal from impurities.[38] The results of ESR and magnetic susceptibility indicate that an unpaired electron on Co^{2+} does not behave as a local magnetic moment. The electrical resistivity of Co(Pc)I increases on lowering the temperature.[38] However, the temperature dependence of the resistivity is not an activation-type. Above 100 K, the conductivity increases almost linearly with temperature.

Quirion et al. investigated the temperature dependence of dc conductivity, microwave conductivity, dielectric constant, and thermoelectric power in detail.[39] They found a phase transition around 50 K. From the thermoelectric power plotted versus inverse temperature, they estimated the activation energy in the high-temperature phase to be 1200 ± 100 K (at 300 K) and that in the low-temperature phase to be 61 ± 2 K (at 60 K). The dielectric constant was 4700 at room temperature, and after a small decrease until 100 K, it dropped suddenly to a value of 580 at low temperatures. The dc and microwave conductivity (Figure 16) exhibited a similar temperature dependence with a positive slope $\delta\sigma/\delta T > 0$ down to 80 K. Since the discrepancy between the two measurements became obvious below 80 K, the charge transport seemed to be dominated by hopping conduction. In contrast with Cu(Pc)I, conductivity change under the applied magnetic field ($B < 10$ T) was not observed in Co(Pc)I.

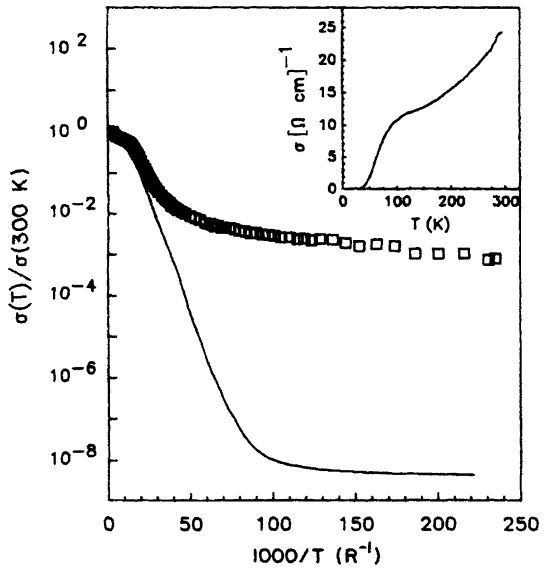

Figure 16. Normalized conductivity of Co(Pc)I as a function of inverse temperature: dc (—) and microwave (15 GHz, □) conductivities. (inset) dc conductivity as a function of temperature on a linear scale. (Reprinted with permission from ref 39. Copyright 1990 American Physical Society.)

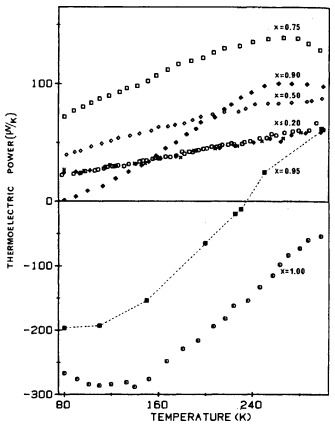

Figure 17. Thermoelectric power of Co_xNi_{1-x}(Pc)I alloys (x = 0.02, 0.10, 0.20, 0.50, 0.75, 0.90, 0.95, and 1.00). For $x < 0.2$, the results are similar to the data for pure Ni(Pc)I ($x = 0$). (Reprinted with permission from ref 40. Copyright 1999 American Chemical Society.)

The crystal structure of Co(Pc)I is similar to that of Ni(Pc)I, and these two salts form alloys Co_xNi_{1-x}(Pc)I. Studies on the magnetic susceptibility, EPR, electrical resistivity, and thermoelectric power were reported for these alloys.[40] Interestingly, the sign of the thermoelectric power changed from negative values to positive ones at $x = 0.95$ (see Figure 17). On the other hand, any corresponding changes on electrical resistivity were not observed. The free-spin-like behavior of the Co d_{z^2} electron was observed only in the vicinity at $x = 0$. Up to composition $x \approx 0.33$, the Curie constant increased with x, although not proportionately; it then decreased with further increase in x, vanishing for Co(Pc)I ($x = 1$). These facts indicate that unpaired electrons on the d_{z^2} orbital couple with each other through the antiferromagnetic interaction. In the Co_xNi_{1-x}(Pc)I alloys with $x \leq 0.75$, a broad EPR signal originating from Co(Pc) was observed. (Co(Pc)I gives no signal at the

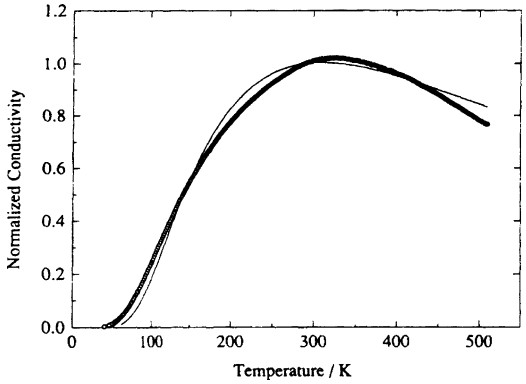

Figure 18. dc conductivity of $(CoPc)_2(AsF_6)$. (Reprinted with permission from ref 41. Copyright 1994 Elsevier Sequoia.)

X-band.) Hyperfine splitting has not been found. The g value abruptly increases with x up to $x = 0.1$ ($x = 0.02$, $g_\perp = 2.34$; $x = 0.10$, $g_\perp = 2.75$) and then gradually decreased. The latter decrease reflects partial oxidation of both the macrocycle π orbitals and the cobalt d_{z^2} orbitals.

2.4.2. $[Co(Pc)]_2(AsF_6)$

This salt has a crystal structure similar to that of Co(Pc)I.[41] However, the average charge density on Co(Pc) is +0.5 in this salt instead of 0.33 in Co(Pc)I. The AsF_6 anions are positionally as well as orientationally disordered. The chemical composition of Co(Pc) and AsF_6 was determined to be 1:0.5 by EPMA analysis of the Co and As atoms. Although the crystal form of $[Co(Pc)]_2(AsF_6)$ (tetragonal) is different from that of $[Ni(Pc)]_2(AsF_6)$ (orthorhombic), these two salts form alloys $[Co_xNi_{1-x}(Pc)]_2AsF_6$. The crystal form of the alloys is orthorhombic for $x < 0.25$ and tetragonal for $x > 0.45$.[42]

Thermoelectric power of $[Co(Pc)]_2(AsF_6)$ is ~50 μV/K around room temperature, almost constant to 50 K, and then drops.[41,43] The dc conductivity[41,43] and microwave conductivity[43] exhibit activation-type temperature dependence (see Figure 18). The magnetic susceptibility is well fitted to $\chi(T) = C/(T - \Theta) + \chi_C$ ($C = 0.052 \pm 0.005$ emu·K·mol^{-1}, $\chi_c = (4.3 \pm 0.1) \times 10^{-4}$ emu·mol^{-1}, $\Theta = -5.2 \pm 0.1$ K), the Curie−Weiss formulas with temperature-independent susceptibility χ_c. The observed Curie constant is approximately 10% of the estimated value for free spins ($C = N\mu_B^2 g^2 S(S + 1)/3k_B$; $g = 2.0023$; $S = 1/2$). This indicates that the magnetic susceptibility is suppressed by an antiferromagnetic interaction.[41]

On the basis of infrared absorption spectra, Yakushi et al. proved that the conduction band in $[Co(Pc)]_2(AsF_6)$ was formed from oxidized π orbitals of the Pc ring.[21] A similar conclusion was given by the optical conductivity spectra in the visible region.[23] This conclusion contrasts with that of Martinsen et al. for Co(Pc)I.[38] Figure 19 shows the reflectance spectra of $[Co(Pc)]_2(AsF_6)$ in comparison with those of $[Ni(Pc)]_2(AsF_6)$. As can be seen from the spectra, both $[Ni(Pc)]_2(AsF_6)$ and $[Co(Pc)]_2(AsF_6)$ exhibit metallic reflection spectra in the infrared region measured. Interestingly, the plasma edge of $[Co(Pc)]_2(AsF_6)$ ($E//c$; ~7500 cm^{-1}) is much higher than that of $[Ni(Pc)]_2(AsF_6)$ ($E//c$; ~5000 cm^{-1}), although the two compounds are expected to have almost the same π-overlapping integral along the 1D axis and the same carrier density. According to Ding et al., this is due the charge-transfer band around 4500 cm^{-1}. This band appears in the $E//c$ spectrum of $[Co(Pc)]_2(AsF_6)$ but is absent in the $E//c$ spectrum of $[Ni(Pc)]_2(AsF_6)$. They attributed this band to the charge-transfer excitation associated with the unpaired electrons on the Co d_{z^2} orbitals.[42] The appearance of this band indicates that there is a strong antiferromagnetic coupling between the Co d_{z^2} orbitals. This conclusion is consistent with the suppression of the magnetic susceptibility in $[Co(Pc)]_2(AsF_6)$. The excitation energy (4500 cm^{-1}, ~ 0.5 eV) of the transition gives a rough estimate for the on-site Coulomb energy of the Co d_{z^2} orbital. Considering a narrow space for an electron on the $3d_{z^2}$ orbital, the estimate seems to be too small. Ding et al. propose that the remarkable reduction of the on-site Coulomb energy of the $3d_{z^2}$ orbital is probably caused by the strong polarization effect by the conjugated π electron in the macrocycle surrounding the Co.[42]

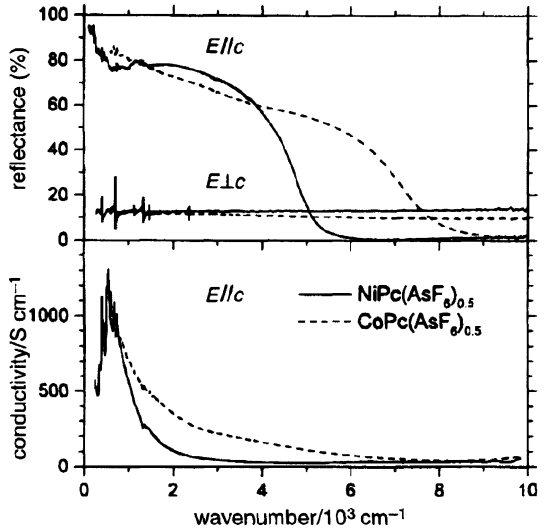

Figure 19. Reflectance spectra (top) and optical conductivity spectra (bottom) of $[Ni(Pc)]_2(AsF_6)$ and $[Co(Pc)]_2(AsF_6)$. (Reprinted with permission from ref 42. Copyright 2001 Royal Society of Chemistry.)

By use of powder absorption spectra in the infrared region and visible region, Yakushi et al. revealed that pressure-induced charge transfer similar to $[Ni(Pc)]_2(AsF_6)$ also existed in $[Co(Pc)]_2(AsF_6)$.[6,19,23,25]

Although no ESR signal was observed in $[Co(Pc)]_2(AsF_6)$, it was possible to observe in $[Co_xNi_{1-x}Pc]_2(AsF_6)$ with $x < 0.09$.[42] Simoniyan et al. measured the ESR spectra of $Co_{0.01}Ni_{0.99}(Pc)(AsF_6)_{0.5}$ and analyzed the spectra (Figure 20) in detail. They succeeded in estimating the exchange interaction between the d_{z^2} electron and π electron as $J_{\pi-d} = 0.013$ eV.[44]

2.5. Pt(Pc) Salts

2.5.1. $[Pt(Pc)]_2(ClO_4)$ and $Pt(Pc)(AsF_6)_x$

Pt(Pc) is synthesized from $PtCl_2$ and phthalonitrile. The crystal form of $[Pt(Pc)]_2(ClO_4)$ is tetragonal, similar to Ni(Pc)I. The AsF_6 salt was considered to

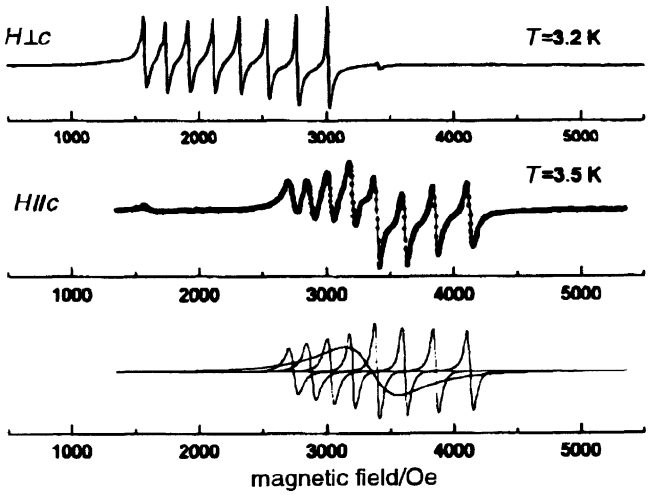

Figure 20. EPR spectra of $[Co_{0.01}Ni_{0.99}Pc]_2(AsF_6)$ alloys. (Reprinted with permission from ref 42. Copyright 2001 Royal Society of Chemistry.)

be isostructural to the ClO_4 salt since the Weissenberg and oscillation photograph of the two salts were the same.[45] Physical properties were mainly reported for the ClO_4 salt. The dc resistivity decreased on lowering the temperature to 100 K. Thus, the crystal is metallic at least to 100 K.[45] The microwave conductivity of the ClO_4 salt increased on lowering the temperature to 150 K and decreased below 150 K.[18] The line width of the ESR spectra followed Elliot's mechanism. The line width decreased on lowering the temperature to 20 K. No symptom of phase transition was observed in the ESR spectra. The spin susceptibility was Pauli paramagnetic to 20 K.[45] On the basis of the XPS and USP spectra, it was concluded that the conduction pathway was located mainly at the ligand chain due to a partial oxidation of the ligand-centered HOMO.[46] The width of the conduction band was estimated to be 1.2 V from the reflectance spectra assuming the Drude model.[45]

2.6. Other Pc Salts Including $M(Pc)_2I_x$

Among the powder iodinated materials of M(Pc) with M = Fe, Co, Ni, Cu, Zn, Pt, and H_2 in the first report,[7] the single-crystal sample was also prepared for Fe(Pc).[47] Crystal growth was attempted by the same method as that for Ni(Pc)I. However, it was rather difficult since the procedure produced a byproduct of the $[Fe(Pc)Cl]_2I_2$ crystals and only a small amount of Fe(Pc)I.[47] The crystal structure is isomorphous with Ni(Pc)I but with a slightly larger interplanar spacing (3.38 Å) compared with other metals. This might be reflected in its conductivity; the room-temperature value was lower than those of other M(Pc)I (20 S cm^{-1}), and the weak metallic temperature dependence was observed only above 200 K. Unfortunately, Fe(Pc)I was ESR silent, and its electronic structure is unknown.

Pc conductors with a similar face-to-face stacking structure were obtained as iodinated salts of sandwich-type $M(Pc)_2$ complexes. The compounds are represented as $M(Pc)_2I_x$, and the valence of M and the iodine content (x) can be varied. As for the M^{III} species, Bi,[48] Yb,[49] As,[49] and In[50] were reported, and for the M^{IV} species, Ti,[51] U,[52,53] and Zr[50] were reported. Though the crystal for M = Ti was obtained by the same method as that for M(Pc)I, the other crystals were obtained by a direct reaction of metal powder, 1,2-dicyanobenzene, and iodine. They have a tetragonal unit cell (Table 1), and the Pc units form one-dimensional columns with I_3^- one-dimensional chains between them. Similar to M(Pc)I, the iodine chain is disordered, since there is no correlation between the iodine chains. The x values so far reported are 3/2, 5/3, and 2, and the iodine arrangement is supposed to be almost the same as that in M(Pc)I when $x = 2$. For the smaller x values, the iodine atoms are deficient. The metal ion in the sandwich-type $M(Pc)_2$ unit can take either of the two different sites between the Pc rings in a column, so that the metals are also disordered as shown in Figure 21. The metals locate at a middle point between the two Pc rings, except for M = Bi and As in which the metals are closer to one of the rings. From the ESR measurements it was confirmed in most cases that the oxidation occurred on the Pc rings.

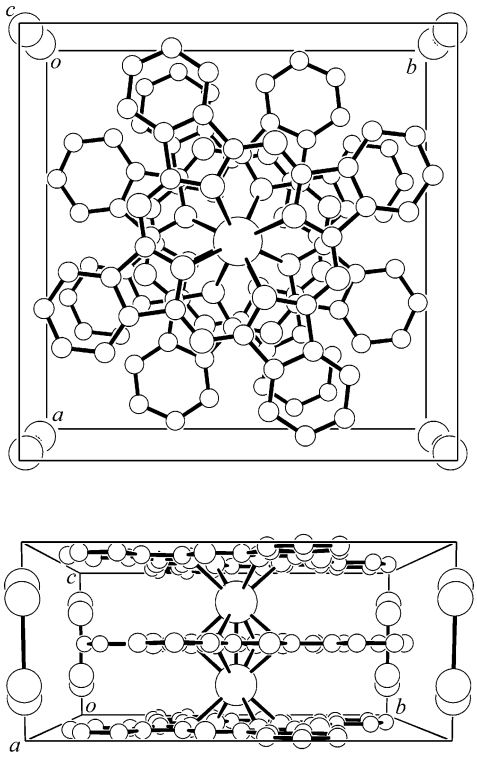

Figure 21. Crystal structure of $Yb(Pc)_2I_2$. The I and Yb atoms are disordered.

The partially oxidized state of the Pc ring varies by the valence of the metal ion and x. For $M^{III}(Pc)_2I_{3/2}$, the Pc ring is oxidized by (3/4)e (M = Bi), for $M^{III}(Pc)_2I_2$, the ring is oxidized by (5/6)e (M = Yb, As, In), for $M^{IV}(Pc)_2I_{5/3}$, the ring is oxidized by (5/18)e (M = U), and for $M^{IV}(Pc)_2I_2$, the ring is oxidized by (1/3)e (M = Ti, U, Zr). In contrast with the Pc rings in the unoxidized $M(Pc)_2$ unit, which are usually largely warped, they become more planar in the iodinated salts; in particular, the rings are almost planar in $U(Pc)_2I_{5/3}$, $In(Pc)_2I_2$, and $Zr(Pc)_2I_2$. The staggering angle between the two overlapping Pc

Chart 2

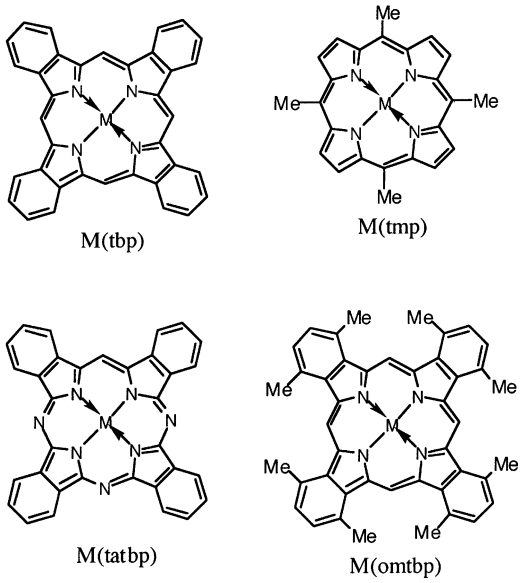

rings is close to those observed for M(Pc)I; the angle is in a range between 40° and 45°. Though it is of a great interest to know how the difference in the partial oxidation state of the Pc ring, that in the Pc ring conformation, and that in the metal species affect the electrical properties, single-crystal conductivity data are unfortunately not available due to their too small crystal sizes. The room-temperature conductivity of the powder compactions is $10^{-4}-10^{-2}$ S cm^{-1}. Since the anisotropy of the conductivity must be rather large, it is necessary to obtain single-crystal data for systematic comparison of these crystals.

3. Face-to-Face-Stacked Partially Oxidized Porphyrin Salts

In one sense, Pc is a chemical modification of porphyrin and can be called tetraazatetrabenzoporphyrin. The molecule in which one nitrogen atom bridging the pyrole rings is replaced by a CH group is triazatetrabenzoporphyrin (tatbp), and that with four CH groups is tetrabenzoporphyrin (tbp). Though the first report on the omtbp conductors appeared at almost the same time as the report on the Pc conductors, we will start with Ni(tbp)I, which has a structure close to that of the typical Pc system of Ni(Pc)I, Chart 2.

3.1. Ni(Tbp)I

Soon after the paper on the single-crystal Ni(Pc)I conductor was published, the structure and physical properties of this compound were published.[54] The crystal growth method was the same as that for Ni(Pc)I. The structural features are also the same as those of Ni(Pc)I; the interplanar spacing between the Ni(tbp) molecules in the one-dimensional column is 3.26 Å, and the molecules have a staggering angle of 41°. The crystal data of the porphyrin conductors are summarized in Table 2. The iodine chain is again constructed by the disordered I_3^- array. The magnetic susceptibility was temperature-independent Pauli-like, and the bandwidth was first reported as 0.44 eV. This value was revised to be 0.22 eV in the report on the high-purity sample.[55] In any way, the values are not much different from that in Ni(Pc)I (0.39 eV). Therefore, this compound is considered to be a metal with a partially oxidized state as $[Ni(tbp)]^{0.33+}(I_3^-)_{0.33}$. In fact, the conductivity at room temperature was 300

Table 2. Space Group, Cell Parameters, and Interplanar Spacing of Porphyrin Conductors

compound	space group	cell parameters	cell volume/Å^3	Z	temp/K	interplanar spacing/Å	ref
Ni(tbp)I	*P*4/*mcc*	a = 14.081(25) Å c = 6.434(11) Å	1276	2	113	3.217	54
Ni(tmp)I	*P*4/*nnc*	a = 16.610(15) Å c = 6.932(7) Å	1913	4	114	3.466	59
Ni(tmp)$(PF_6)_{0.5}$	*P*4/*nnc*	a = 16.685(1) Å c = 6.994(1) Å	1947	4	220	3.497	60
Ni(tmp)$(ReO_4)_{0.5}$	*P*4/*n*	a = 16.710(4) Å c = 6.720(2) Å	1876	4	125	3.355 3.365	61
Cu(tatbp)I	*P*4/*mcc*	a = 13.998(5) Å c = 6.426(3) Å	1259	2	120	3.213	63
Co(tbp)I	*P*4/*mcc*	a = 14.129(3) Å c = 6.334(1) Å	1249	2	125	3.167	29
Cu(tmp)$(ReO_4)_{0.5}$	*P*4/*n*	a = 16.774(9) Å c = 6.746(4) Å	1898	4	110	3.369 3.377	65
Pd(tmp)$(ReO_4)_{0.5}$	*P*4/*n*	a = 16.778(6) Å c = 6.723(3) Å	1892	4	110	3.371 3.375	66
Ni(omtbp)$I_{1.08}$	$P4_2/nbc$	a = 21.011(9) Å c = 7.556(5) Å	3335.5	4		3.778	68
$[Cu(tatbp)]_3(ReO_4)_2C_{10}H_7Cl$	$P\bar{1}$	a = 9.167(6) Å b = 15.849(10) Å c = 16.065(10) Å α = 65.87(2)° β = 72.11(3)° γ = 84.01(2)°	2126	1	110	3.190 3.482	69
$[Ni(tbp)]_3(AsF_6)_2C_{10}H_7Cl$	$P\bar{1}$	a = 16.019(2) Å b = 16.470(3) Å c = 9.853(5) Å α = 103.30(2)° β = 96.10(3)° γ = 66.06(1)°	2255	1		3.221 3.608	70

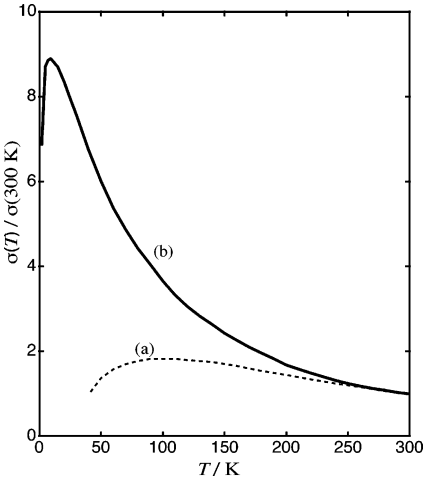

Figure 22. Temperature dependence of the conductivities of Ni(tbp)I. The conductivity data are replotted: (a) ref 54 and (b) ref 55 (purest sample).

S cm^{-1} and increased with decreasing temperature. In the first paper[54] the conductivity showed a broad maximum at 95 K (Figure 22a). After preparing high-purity crystals, it was found that this crystal retained high conductivity to low temperature as found for Ni(Pc)I (Figure 22b); the maximum shifted to 9 K, and the maximum value increased to 9 times the room-temperature value (1.8 times in ref 54). The downturn in the conductivity below 9 K, which was also observed in very pure Ni(Pc)I below 5 K, was supposed to be due to localization effects.

This improvement of the sample quality not only improved the transport properties but also affected the interpretation of the conduction mechanism. The structure of tbp is closely related to that of Pc, but there is a difference in the electronic structure. In the case of Pc, the energy difference between the a_{1u} HOMO and a_{2u} NHOMO is substantially large, while it is nearly degenerate in the unsubstituted porphyrin π system. In the tbp π system the energy difference is not as small but surely smaller than that in the Pc π system. In contrast to a_{1u} HOMO, a_{2u} NHOMO may have a possibility of mixing with the d orbitals of the central metal. Therefore, if holes can transfer from the π system to a d orbital, "doubly mixed valency" in which both π and d orbitals are included in the partial oxidation would become possible. In the first report this possibility was suggested from the temperature dependence of the g factor of the ESR signal.[54,56−58] However, this idea was abandoned after measurement of the pure sample; the compound was found to be a pure π-electron conductor since there was no indication of the existence of Ni^{3+} in the ESR signal.

3.2. Ni(Tmp)X_y

The tmp ligand can be constructed from tbp by removing the peripheral benzo groups and replacing the bridging CH portions to the C-Me groups. This modification is supposed to make a large difference from the Pc ligand not only in the molecular shape but also in the electronic structure.

3.2.1. Ni(tmp)I

Single crystals of Ni(tmp)I were grown by slow diffusion method at room temperature using benzene as the solvent.[59] The absence of the peripheral benzo groups in tmp made the crystal structure different from the Pc conductors. However, the crystal has many common features found in the Pc systems. The crystal system is tetragonal (space group *P*4/*nnc*), and the Ni(tmp) molecules are stacked by the metal-over-metal fashion, as shown in Figure 23a. Also the

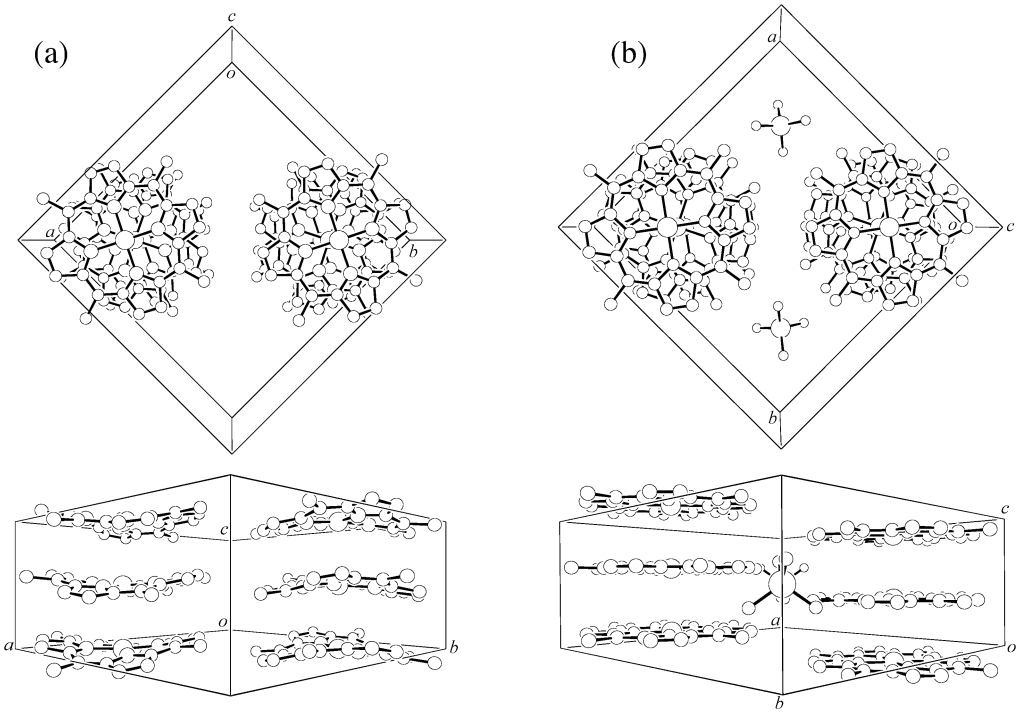

Figure 23. (a) Crystal structure of Ni(tmp)I. The iodine chains (run at (1/4, 1/4, z) and (3/4, 3/4, z)) are omitted. (b) Crystal structure of Ni(tmp)$(ReO_4)_{0.5}$.

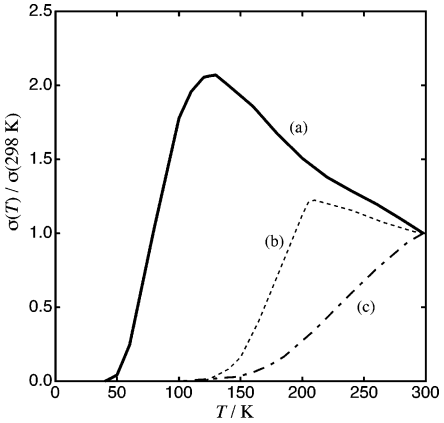

Figure 24. Temperature dependence of the conductivities of (a) Ni(tmp)I [ref 53], (b) Ni(tmp)$(PF_6)_{0.5}$ [ref 54], and (c) Ni(tmp)$(ReO_4)_{0.5}$ [ref 55]. The conductivity data are replotted.

iodine chain is constructed by the I_3^- species and surrounded by the one-dimensional columns of Ni(tmp). However, a notable difference was found in the molecular planarity; Ni(tmp) is deformed in the S_4-ruffled shape. This made the Ni···Ni distance between the neighboring molecules in the column larger in Ni(tmp)I (3.446 Å) than in Ni(Pc)I by 0.2 Å. The staggering angle between the overlapped molecules is 37°. The conductivity at room temperature is 110 S cm^{-1} and increased with decreasing temperature down to 115 K (Figure 24a). Below this temperature the conductivity decreased gradually and finally becomes an insulator at the lowest temperature. The paramagnetic susceptibility was temperature independent from room temperature to 28 K; then the susceptibility decreased abruptly. Therefore, the transition into a diamagnetic ground state is considered to occur at this temperature. The temperature-independent paramagnetic component is rather large as a Pauli-like paramagnetism and suggests the larger on-site Coulomb repulsion energy due to a small size of the π-ligand in Ni(tmp). The possibility that the nearly degenerate HOMO and NHOMO might cause triplet contribution was suggested.

3.2.2. Ni(tmp)$(PF_6)_{0.5}$

Single crystals of Ni(tmp)$(PF_6)_{0.5}$ were obtained by electrolysis in 1,1,2-trichloroethane.[60] The diffraction data taken at 220 K indicated that the crystal is isomorphous with Ni(tmp)I. However, the PF_6^- anion is ordered in the channel surrounded by the Ni(tmp) columns. Overlapping two S_4-ruffled Ni(tmp) molecules are separated by 3.497 Å and have a staggering angle of 34.7°. The conductivity at room temperature was 100 S cm^{-1} and showed metallic behavior down to 205 K (Figure 24b). Below this temperature the conductivity decreased rather rapidly, but the diffraction data at 150 K revealed no indication of the structural transition. The paramagnetic susceptibility contained both temperature-independent and Curie-like components. It is rather curious that the Curie-like component is large (corresponding to 22% of the Ni(tmp) molecules).

3.2.3. Ni(tmp)$(ReO_4)_{0.5}$

Single crystals of Ni(tmp)$(ReO_4)_{0.5}$ were obtained by the same method for the PF_6 salt. The crystal system is again tetragonal but with lower symmetry (space group $P4/n$; Figure 23b).[61] The molecular arrangement is basically the same as those in the other salts. Ni(tmp) in this salt is planar, and the interplanar distance is 3.355 Å. The staggering angle in the one-dimensional column is 27.5°. Since ReO_4^- anion lies on a site crystallographically imposed $\bar{4}$ symmetry, no orientational disorder occurs. Though due to the crystal symmetry, there are two crystallographically distinct Ni(tmp) molecules; they are virtually in the same circumstances and do not have a dimerized structure. The conductivity at room temperature was 90 S cm^{-1}, which was not much different from those of the other salts, but the temperature dependence was found to be semiconducting (Figure 24c). The paramagnetic susceptibility contained both temperature-independent and Curie-like components as found for the PF_6 salt. The Curie component in the ReO_4 salt was reasonably small as defects or impurities.

Comparison of the above three salts indicates a systematic narrowing of the metallic temperature region from Ni(tmp)I to Ni(tmp)$(PF_6)_{0.5}$ to Ni(tmp)$(ReO_4)_{0.5}$. The most important parameter in this systematic change was thought to be the staggering angle.[61] In the simple porphyrin without any substituents, the a_{1u} and a_{2u} orbitals are nearly degenerate. It was predicted that the overlap integral of the a_{1u} orbital between the π ligands becomes maximal when the staggering angle is 0° and 45° and becomes 0 at 19°.[62] On the other hand, the maximum overlap integral value of the a_{2u} orbital is attained when the angle is 0, and the overlap integral continuously decreases with increasing the angle from 0° to 45°. Therefore, the systematic narrowing of the metallic region from a staggering angle of 37° in Ni(tmp)I to that of 27.5° in Ni(tmp)$(ReO_4)_{0.5}$ may be related to the systematic decrease of the bandwidth composed of the a_{1u} orbitals.

3.3. Cu(Tatbp)I

Cu(tatbp) has an unpaired electron on the Cu $d_{x^2-y^2}$ orbital. In a charge-transfer salt of Cu(tatbp), the π orbital of tatbp is expected to form the conduction band and an unpaired electron on the $d_{x^2-y^2}$ orbital is expected to behave as a local magnetic moment. Thus, interplay between the conduction electrons and local magnetic moments is expected in a charge-transfer salt containing Cu(tatbp). This situation is analogous to that in Cu(Pc)I.

Cu(tatbp)I has a crystal structure similar to Cu(Pc)I.[63] The magnetic susceptibility of this salt is expressed as $\chi(T) = \chi_{Cu}(T) + \chi_{Pauli} = C/(T - \theta) + \chi_\pi$, with $C = 0.428$ emu·K·mol^{-1}, $\theta = -6.9$K, and $\chi_\pi = 2.8 \times 10^{-4}$ emu·mol^{-1}. The values of these parameters are close to those of Cu(Pc)I. The Curie constant estimated using the parameters $g_{av}^2 = 4.382$ (the averaged square of g value) and $S = 1/2$ is 0.406 emu·K·mol^{-1}. The consistency in the observed and estimated values demonstrates that the unpaired

electron on the Cu $d_{x^2-y^2}$ behaves as a local magnetic moment.[63]

The g value of Cu(tatbp)I at room temperature is $g_{\parallel} = 2.148$ and $g_{\perp} = 2.036$. On lowering the temperature, the g value shifts upward. This is due to the exchange coupling between the π-conduction electrons and unpaired $d_{x^2-y^2}$ electrons that behave as local magnetic moments. Similar to Cu(Pc)I, an anomalous increase of the g value and line width was observed in the X-band ESR below $T_b = 6-8$ K. The discrepancy between the microwave conductivity and dc conductivity, a decrease of microwave conductivity under magnetic field, was observed below T_b in Cu(tatbp)I.[63,64] These unusual phenomena are very similar to those observed in Cu(Pc)I (see section 2.3 and Figure 12).

3.4. Co(Tbp)I

To compare with Co(Pc)I, Co(tbp)I was investigated.[29] Though they are isomorphous with each other, the electronic structure is supposed to be different; in contrast with the possibility of metal oxidation in Co(Pc)I, ligand oxidation occurs in Co(tbp)I due to the smaller ionization potential of tbp than Pc. The conductivity was 500 S cm^{-1} at room temperature and showed metallic behavior down to 170 K. Below this temperature the conductivity gradually decreased. The thermoelectric power was metallic down to 90 K. The bandwidth estimated from the TEP was 1.3 eV. The Curie-like susceptibility component was much smaller than that expected from the localized spins in Co^{2+} atoms (about one-tenth of the full value). It was considered that spins in Co^{2+} d_{z^2} orbitals were strongly antiferromagnetically coupled due to the orbital overlaps. This was consistent with the absence of the magnetoresistance. The relatively high temperature of the maximum conductivity was thought to be due to the localized magnetic moments.

3.5. $[M(Tmp)]_2(ReO_4)$

The compounds which belong to this category are $[Cu(tmp)]_2(ReO_4)$ and $[Pd(tmp)]_2(ReO_4)$, and they have the same crystal structure as the Ni salt in section 3.2.

3.5.1. $[Cu(tmp)]_2(ReO_4)$

The conductivity behavior of the Cu salt resembled that of the Ni salt; the room temperature value was 40 S cm^{-1}, and the temperature dependence was semiconducting.[65] Though the Cu−Cu magnetic exchange mediated by the π-electron system operated as in Cu(Pc)I, the temperature dependence became exponential, which was linear in Cu(Pc)I. This is due to its thermally activated conductivity, and the coupling was thus weakened with decreasing temperature ($\theta = -3.1$ K). Since the angle dependence of the line width of the ESR signal showed typical one-dimensional behavior, the coupling was restricted in the 1D chain.

3.5.2. $[Pd(tmp)]_2(ReO_4)$

All the structural and physical properties of the Pd salt were similar to those of the Ni salt. The conductivity at room temperature was 30 S cm^{-1} and showed semiconducting behavior.[66] The Pd salt revealed temperature-independent paramagnetism similar to the Ni salt. The origin was interpreted as Van Vleck paramagnetism.

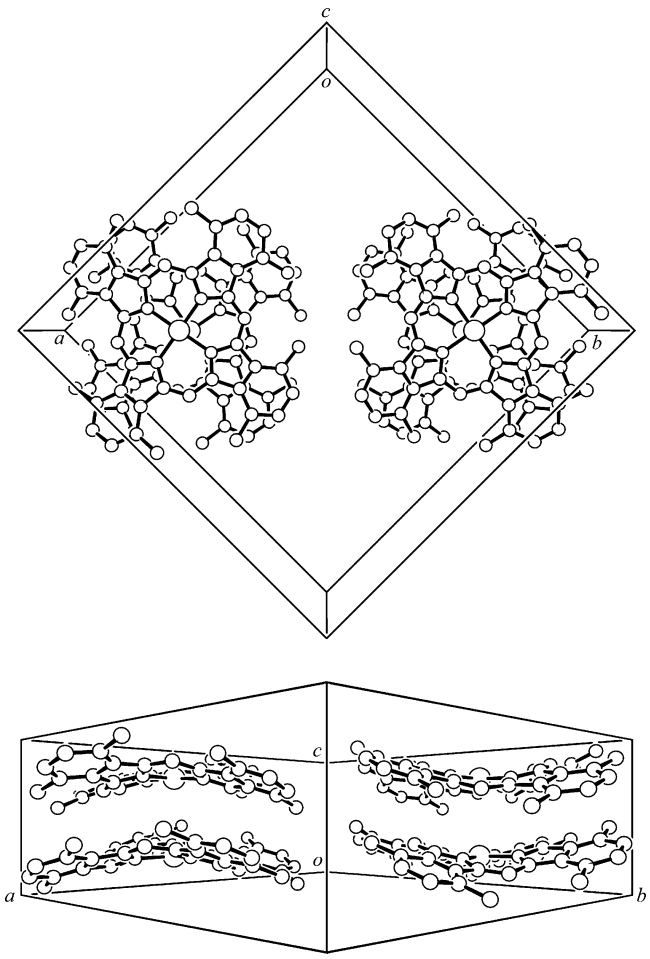

Figure 25. Crystal structure of $Ni(omtbp)I_{1.08}$. The iodine chains (run at (1/4, 1/4, z) and (3/4, 3/4, z)) are omitted.

3.6. Other Porphyrin Salts

$Ni(omtbp)I_x$ (omtbp = octamethyltetrabenzoporphyrin) with $x = 1.08$ and 2.9 were the first porphyrin conductors reported.[67] When crystal growth was performed with chlorobenzene, in addition to the needle crystals of $x = 1.08$, needles of $x = 2.9$ were obtained. Structural analysis was carried out only for the crystal of $x = 1.08$; the crystal system was tetragonal with the space group $P4_2/nbc$.[68] The Ni(omtbp) molecule was severely ruffled due to the steric interaction between the eight methyl groups as shown in Figure 25. The molecular stacking was however a metal-over-metal type, forming a 1D column. The Ni···Ni distance (3.778 A) in the column is rather long due to nonplanarlity. The staggering angle is 40°. The chemical species of the iodide was I_3^- in both salts. It is aligned as a chain in the channel surrounded by the Ni(omtbp) columns in the crystal of $x = 1.08$. The oxidation states were, therefore, represented as $[Ni(omtbp)]^{+0.36}(I_3^-)_{0.36}$ and $[Ni(omtbp)]^{+0.97}(I_3^-)_{0.97}$. In both salts the g factor of the ESR spectra indicated that the unpaired electron existed in the π ligand. The conductivity at room

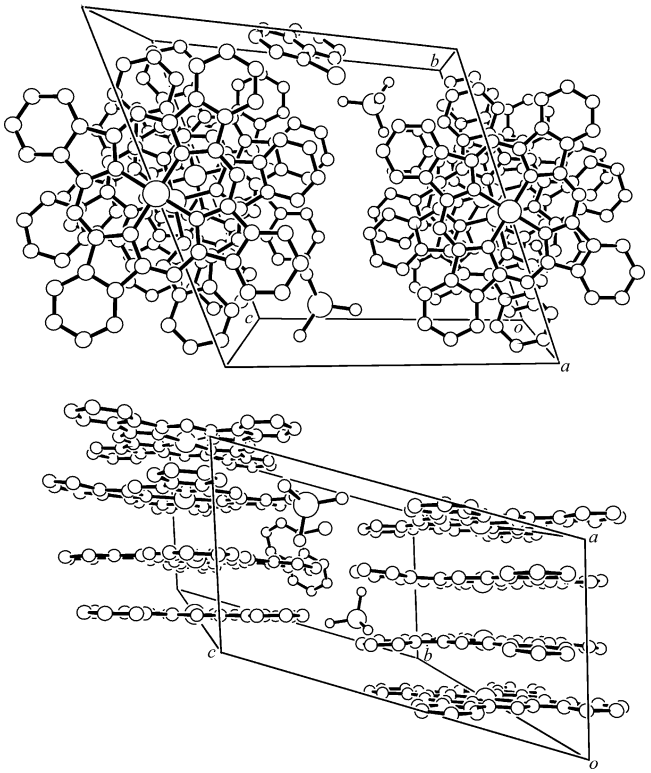

Figure 26. Crystal structure of $[Cu(tatbp)]_3(ReO_4)_2 \cdot C_{10}H_7Cl$. Only one-half of disordered 1-chloronaphthalene is shown.

temperature was 10 S cm^{-1}, and the metallic behavior was observed only above 300 K. Since the bandwidth is small due to the large interplanar spacing, the magnetic susceptibility was Curie-like, indicating localizing spins. The conductivity of the crystal with $x = 2.9$ was 3 S cm^{-1} at room temperature and semiconducting. The susceptibility at room temperature was nearly of localizing spins, but the temperature dependence deviated from the ideal Curie behavior.

As the ReO_4 salts of the tatbp complexes, $[Ni(tatbp)]_3[ReO_4]_2 \cdot C_{10}H_7Cl$ and $[Cu(tatbp)]_3[ReO_4]_2 \cdot C_{10}H_7Cl$ were reported.[69] They are isomorphous with each other; the crystal system is triclinic, and the structure is considerably different from the other porphyrin conductors (Figure 26). The most notable feature is the trimerized unit in the column; the M···M distance within the trimer is much smaller than that between the trimers (3.190 vs 3.482 Å in the Cu salt). Though the π ligand was formally in the partially oxidized state, charge transport was of semiconducting behavior with 10^{-4} S cm^{-1} at room temperature due to gap formation resulting from the trimerized structure. The magnetic susceptibility of the Cu salt was a Curie−Weiss type with a Weiss temperature of −5.2 K. This was speculated as valence band electron mediated coupling in the trimer. Since the hyperfine structure could be observed in the Cu−Ni alloy system, it was suggested that the Cu−Cu spin exchange mediated by the polarization of the electrons in the nonbonding band operated. $[Ni(tbp)]_3(AsF_6)_2 \cdot C_{10}H_7Cl$ was known as the compound having the crystal structure similar to $[Cu(tatbp)]_3[ReO_4]_2 \cdot C_{10}H_7Cl$. This salt showed the same semiconducting behavior (10^{-3} S cm^{-1} at room temperature).[70]

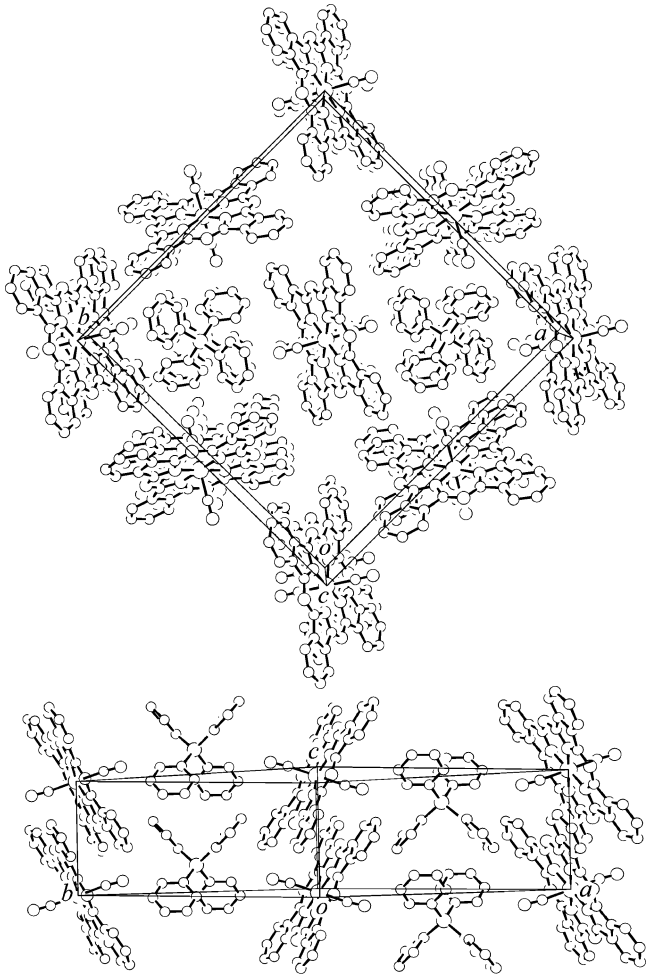

Figure 27. Crystal structure of $TPP[Co(Pc)(CN)_2]_2$.

4. Slipped-Stacked Partially Oxidized Phthalocyanine Salts

Axially substituted Pc compounds have been utilized for construction of conductors with slipped $\pi-\pi$ stacks. These Pc compounds are mainly with Co^{III} or Fe^{III}, and the molecules are no longer planar. To date the best studied compound in this class is $[Co^{III}(Pc)(CN)_2]^-$, which includes nonmagnetic Co^{III}. The π ligand of this parent compound is oxidized, and conducting charge-transfer salts are formed. The anion $[Co^{III}(Pc)(CN)_2]^-$ was originally designed for the precursor of the CN-bridged polymer.[71] In 1985 it was reported that conducting crystals could be obtained by electrolysis of the potassium salt in acetonitrile.[72−74] In this report the structural analysis was unsuccessful, and it was speculated that the five-coordinate $Co^{III}(Pc)CN$ molecules constructed the crystal. It was rather doubtful that the high conductivity was realized in the crystal composed of the closed-shell π-ligand compounds. The structure of the product of the electrolysis was solved in 1989.

Galvanostatic electrolysis of $K[Co^{III}(Pc)(CN)_2]$ in acetonitrile gave rodlike crystals on the anode surfaces.[75,76] The crystals are thicker than needles of the $M(Pc)X_y$-type conductors. However, it was found under the microscope that the crystal shape was gradually deformed after isolating the crystals from the electrochemical cell. This was thought to relate

Chart 3

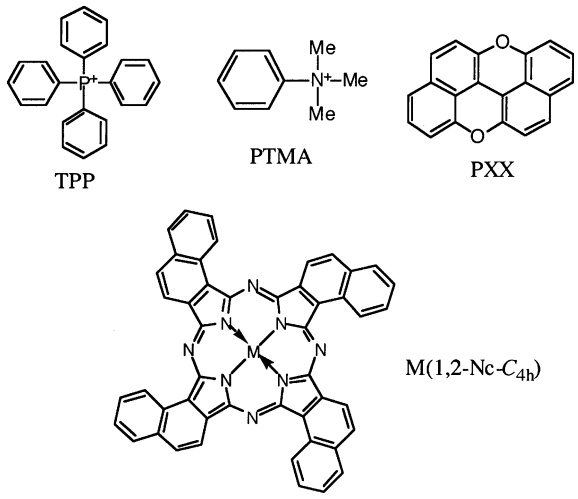

to the fact that the structural analysis was unsuccessful and the diffraction measurements were performed using a crystal sealed in a capillary with the mother solution. The composition of the crystal was found to be $K[Co^{III}(Pc)(CN)_2]_2 \cdot 5CH_3CN$, and it became clear that the Pc ring was partially oxidized by 0.5e. Also, it was found that the Bragg diffraction peaks were not observable when the crystal was exposed to air due to the mosaic distortion of the crystal by exclusion of acetonitrile. The Pc rings form slipped stacks, constructing a two-dimensional sheet. This structural motif provided a clue to the development of conductors with various stacking structures based on the $Co(Pc)(CN)_2$ unit.[77,78]

The starting anion, $[Co^{III}(Pc)(CN)_2]^-$, can easily be prepared by air oxidation of $Co^{II}(Pc)$ under coexistence of CN^-.[71] In this system magnetic moments can be introduced by replacing the central Co^{III} by Fe^{III}. The preparation of $[Fe^{III}(Pc)(CN)_2]^-$ was found to be not as easy that of $[Co^{III}(Pc)(CN)_2]^-$; the similar method gave $[Fe^{II}(Pc)(CN)_2]^{2-}$. The starting $[Fe^{III}(Pc)(CN)_2]^-$ was obtained by chemical oxidation of $[Fe^{II}(Pc)(CN)_2]^{2-}$. This Fe system may correspond to the face-to-face-stacked $M(Pc)X_y$ system with M = Cu, and details of the effects to the physical properties are described in section 4.4.

When the Pc ring is completely oxidized, the products become neutral radical crystals. They are relatively highly conducting, and their structures and properties are described in section 5.3.

The component molecules in this section are shown in Chart 3.

4.1. $TPP[M(Pc)(CN)_2]_2$

Though $K[Co^{III}(Pc)(CN)_2]_2 \cdot 5CH_3CN$ was a partially oxidized salt, its intrinsic physical properties were not possible to be measured due to its instability. Then the search for other cationic components that can give a partially oxidized salt was carried out. As a result, TPP was found as the earliest cation that gave a partially oxidized salt.

Single crystals can be obtained by electrolysis of the simple salt, $TPP[Co^{III}(Pc)(CN)_2]$, in acetonitrile.[79] The crystal system is tetragonal, and the Pc rings are stacked to form a 1D chain (see Figure 27). The TTP cations are also aligned in a 1D chain structure, making the phenyl rings parallel to the Pc planes. Such a tendency of 1D alignment of TPP was reported,[80] and this arrangement may regulate the Pc arrangement. The ratio of cation to anion is 1:2; thus, the Pc ring is formally oxidized by 0.5e. Since the neighboring $Co(Pc)(CN)_2$ units in the chain are related by a simple translation of the unit length of the *c* axis, the chain structure is completely uniform. Therefore, it is expected that HOMOs of the Pc rings form a three-fourths filled metallic band.

The report on $TPP[Fe^{III}(Pc)(CN)_2]_2$ was published 2 years after that of $TPP[Co^{III}(Pc)(CN)_2]_2$.[81] This salt is isostructural with $TPP[Co^{III}(Pc)(CN)_2]_2$. Table 3 summarizes the lattice constants and overlap inte-

Table 3. Space Group and Cell Parameters of the $M(Pc)(CN)_2$ Conductors

compound	space group	cell parameters	cell volume/Å^3	Z	temp/K	overlap integral	ref
$TPP[Co(Pc)(CN)_2]_2$	$P4_2/n$	a = 21.676(8) Å c = 7.474(4) Å	3511	2	296	8.5×10^{-3}	79
$TPP[Fe(Pc)(CN)_2]_2$	$P4_2/n$	a = 21.722(2) Å c = 7.448(2) Å	3514	2	293	8.7×10^{-3}	81
$[PTMA]_x[Co(Pc)(CN)_2] \cdot y\ (CH_3CN)$	$Pnnm$	a = 13.871(1) Å b = 7.350(1) Å c = 16.296(1) Å	1661	2	295	9.4×10^{-3}	90
$[PTMA]_x[Fe(Pc)(CN)_2] \cdot y\ (CH_3CN)$	$Pnnm$	a = 13.900(1) Å b = 7.332(1) Å c = 16.317(1) Å	1663	2	295	10.0×10^{-3}	90
$[PXX][Co(Pc)(CN)_2]$	$P2_1/a$	a = 17.743(2) Å b = 29.344(3) Å c = 7.678(3) Å β = 102.36(2)°	3904	4	293	6.7×10^{-3} (//leg) 2.8×10^{-3} (//rung)	96
$[PXX][Fe(Pc)(CN)_2]$	$P2_1/a$	a = 17.825(3) Å b = 29.397(4) Å c = 7.680(4) Å β = 102.29(3)°	3932	4	293	$6.6\ 10^{-3}$ (//leg) 2.7×10^{-3} (//rung)	97
$[PXX]_2[Co(Pc)(CN)_2]$	$P\bar{1}$	a = 9.893(1) Å b = 18.175(2) Å c = 7.295(1) Å α = 95.18(1)° β = 104.34(1)° γ = 96.41(1)°	1253	1	123	9.9×10^{-3} (//c) 1.8×10^{-3} (//[101])	98

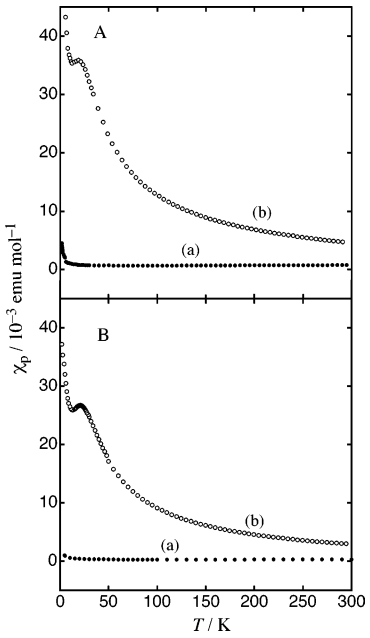

Figure 28. Temperature dependence of the magnetic susceptibility of the randomly oriented polycrystalline sample: (A) TPP[M(Pc)(CN)$_2$]$_2$ and (B) [PTMA]$_x$[M(Pc)(CN)$_2$]·y(CH$_3$CN). In each panel a is M = Co and b is M = Fe.

grals of these two salts. One feature of interest in the physical studies on these salts is that the Fe^{III}(Pc)(CN)$_2$ unit has a local magnetic moment while Co^{III}(Pc)(CN)$_2$ does not. This relation is very similar to that of Cu(Pc)I and Ni(Pc)I. The interplay between the conduction electrons and local magnetic moments is expected in TPP[Fe^{III}(Pc)(CN)$_2$]$_2$.

The magnetic susceptibility of TPP[Co^{III}(Pc)(CN)$_2$]$_2$ was temperature independent and Pauli-like (Figure 28A(a)). However, the bandwidth estimated from this value (7.7×10^{-4} emu mol^{-1}) based on a one-dimensional tight-binding band model is less than 0.2 eV. This width may be too small, and the paramagnetism was considered to be enhanced by the on-site Coulomb repulsion U. Contrary to TPP[Co^{III}(Pc)(CN)$_2$]$_2$, TPP[Fe^{III}(Pc)(CN)$_2$]$_2$ exhibited a Curie−Weiss-type temperature dependence of the magnetic susceptibility at temperatures above ~20 K (Figure 28A(b)).[82] Below 20 K, the susceptibility showed an anomaly, and spontaneous magnetization appears below 6 K.[82,83] The magnetic torque measurement gave additional information on the magnetic properties. Since TPP[Fe^{III}(Pc)(CN)$_2$]$_2$ is isotropic within the ab plane, the torque should be constant for the magnetic field rotated within the ab plane as far as there is no magnetic order. However, the torque exhibited variance below 12 K with the 4-fold symmetry for the magnetic field rotated within the ab plane.[84] This proved that a static magnetic order appeared below 12 K. This magnetic order is associated with the anomalous temperature dependence of the susceptibility below 20 K. The anisotropic behavior of the susceptibility originates from the g-factor anisotropy of the Fe^{III}(Pc)(CN)$_2$ unit.[85] As for this g-factor anisotropy, detailed discussion will be given in section 4.4.

The reflectance spectra of the Fe and Co salts were very similar in shape and highly anisotropic for the

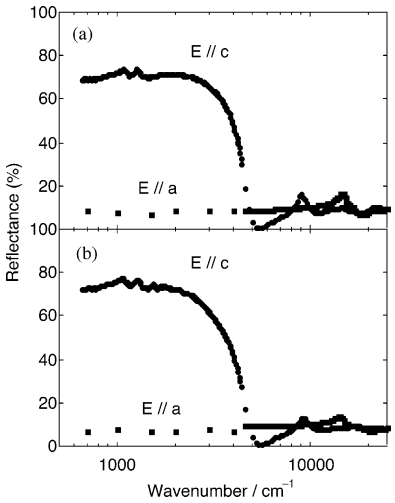

Figure 29. Single-crystal reflectance spectra of (a) TPP[Co(Pc)(CN)$_2$]$_2$ and (b) TPP[Fe(Pc)(CN)$_2$]$_2$.

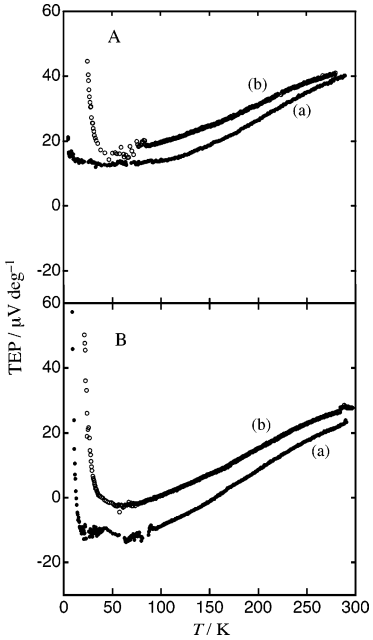

Figure 30. Temperature dependence of the thermoelectric power (TEP) along the Pc stacking direction: (A) TPP[M(Pc)(CN)$_2$]$_2$ and (B) [PTMA]$_x$[M(Pc)(CN)$_2$]·y(CH$_3$CN). In each panel a is M = Co and b is M = Fe.

polarization directions, as shown in Figure 29. This indicates that the π-conduction bands of these two salts are essentially the same. The bandwidth estimated from the plasma frequency of the spectrum polarization parallel to the c axis was 0.62 eV for the Co salt and 0.55 eV for the Fe salt. These values are consistent with those estimated from the slope of the metallic temperature dependence of the thermoelectric power, $4t = 0.5$ eV (almost the same values for both salts).

The Co and Fe salts exhibit a similar temperature dependence of thermoelectric power (Figure 30A). Above 100−120 K the thermoelectric power decreased almost linearly on lowering the temperature. Below 120 K the thermoelectric power of the Co salt became flat and slightly increased at lower temperature.[86] The thermoelectric power of the Fe salt abruptly increased below ca. 45 K.

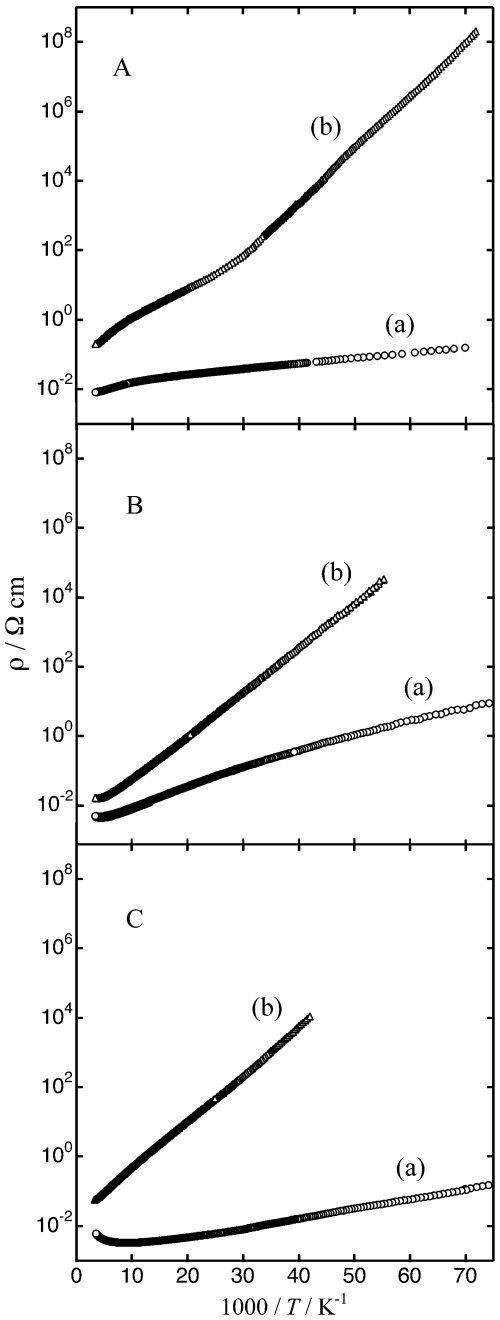

Figure 31. Temperature dependence of the electrical resistivity along the Pc stacking direction: (A) TPP[M(Pc)-(CN)$_2$]$_2$, (B) [PTMA]$_x$[M(Pc)(CN)$_2$]·y(CH$_3$CN), and (C) [PXX]-[M(Pc)(CN)$_2$]. In each panel a is M = Co and b is M = Fe.

Contrary to the similar temperature dependence of the thermoelectric power, the electrical conductivity exhibited very different temperature dependences in these salts. The conductivity of the Co salt at room temperature was approximately 120 S cm^{-1}. The conductivity exhibited an almost constant temperature dependence around room temperature and gradually decreased on lowering the temperature (Figure 31A(a)). The temperature dependence of the conductivity at low temperatures does not fit to the thermally activated behavior. In contrast with the metallic conductivity of the Co salt around room temperature, the conductivity behavior of the Fe salt was semiconducting in the entire temperature range (Figure 31A(b)). The activation energy was estimated to be 0.023 eV at 150 K, 0.016 eV at 55 K, and 0.030 eV at 30 K.

Although reflectance spectra of the Fe and Co salts as well as the thermoelectric power of them are very similar to each other, temperature dependences of the resistivity are very different in these salts. Since the Fe^{III}(Pc)(CN)$_2$ unit has a local magnetic moment, this difference was considered to be due to the interaction between the local magnetic moments and conduction electrons. To examine this in detail, magnetotransport studies were performed. The study showed that the resistivity of the Fe salts at 20 K reduced to a value less than 10% of the zero-field value at $B = 18$ T[82] and less than 1% of the value at $B = 38$ T.[87] This phenomenon is considered to be due to suppression of the magnetic scattering under the high magnetic field. The resistivity decease is larger for $B//a$ than for $B//c$, this is due to the g-factor anisotropy and orientation of the Fe^{III}(Pc)(CN)$_2$ unit (see section 4.4).

The Co salt has strong one-dimensionality ($\sigma_{\parallel}/\sigma_{\perp} = 10^3$) and no local magnetic moment. In this sense, this salt seems to be an ideal one-dimensional conductor. However, electrical properties of this salt are very much different from those of (TMTTF)$_2$X and M(Me$_2$DCNQI)$_2$ (M = Ag and Li), well-known one-dimensional conductors.[88] As we examine the thermoelectric power and magnetic susceptibility, it seems that no energy gap is open in this salt even at low temperatures. Meanwhile, the temperature dependence of the electrical resistivity is not that of typical metals. According to Hasegawa et al., the temperature dependence of the conductivity could be varied by the quality of the crystal as observed for Ni(Pc)I. Interestingly, this salt exhibited large positive magnetoresistance at low temperature ($\Delta R/R \approx 10$ at 2 K).[89] The field dependence of the positive magnetoresistance was almost the same for $B//a$ and $B//c$ below ca. 10 T. In the case of low-dimensional conductors, positive magnetoresistance is highly anisotropic for the field orientation. This comes from the Lorentz force affected by the anisotropic Fermi velocity. In this sense, the observed field-orientation dependence of the positive magnetoresistance in the Co salt seems to be anomalous. More detailed studies are necessary in order to clarify the origin.

TPP[Fe(Pc)(CN)$_2$]$_2$ and TPP[Co(Pc)(CN)$_2$]$_2$ form alloys. In these alloys the transition temperature into a magnetic state (20 K in TPP[Fe(Pc)(CN)$_2$]$_2$) went down. The negative magnetoresistance of the alloys was smaller than that of TPP[Fe(Pc)(CN)$_2$]$_2$.[89] However, the magnetic transition as well as a spontaneous magnetization was still observed in the sample with $x = 0.07$.[83] X-band ESR signal was observed in neither TPP[Fe(Pc)(CN)$_2$]$_2$ nor alloys. These facts indicate that a spin−spin interaction is not negligible even in the alloys with reduced spin concentration.[83]

4.2. [PTMA]$_x$[M(Pc)(CN)$_2$]·y(Solvent)

Electrochemical oxidation of a simple salt of PTMA[M^{III}(Pc)(CN)$_2$] in acetonitrile or acetone was found to yield needlelike crystals on the anode surfaces.[90] The crystal structure is shown in Figure 32. Though at a glance the stoichiometry appears to be 1:1, the solvent molecules have been found to

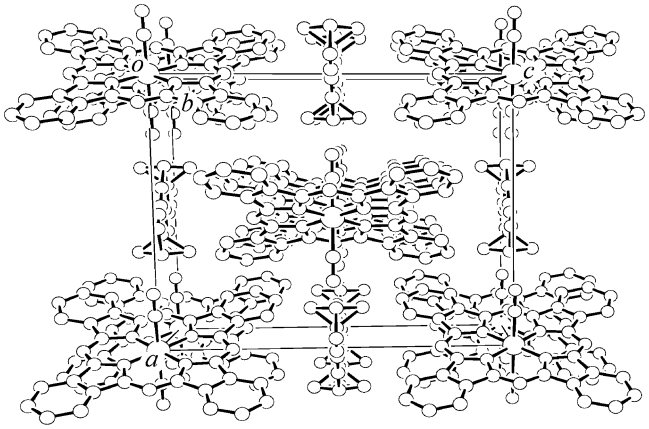

Figure 32. Crystal structure of $[PTMA]_x[Co(Pc)(CN)_2]\cdot y(CH_3CN)$.

partially occupy the cation sites by difference syntheses. Site occupancies of $x = 0.5$ and $y = 1$ were suggested from the final temperature parameters and the slope of the temperature dependence of the thermoelectric power. The $M(Pc)(CN)_2$ units form a one-dimensional chain along the *b* axis.

The temperature dependence of the electrical resistivity for M = Co was similar to that of $TPP[Co(Pc)(CN)_2]_2$: weak metallic behavior around room temperature and gradual increase of the resistivity at lower temperature. For M = Fe, the room temperature value is about one order larger than that for M = Co, and the resistivity increased more rapidly at low temperature (Figure 31B). From the relatively good linear correlation between log ρ of the M = Fe salt and $1/T$, the activation energy was calculated to be 0.024 eV. The temperature dependence of the thermoelectric power was also similar to the $TPP[M(Pc)(CN)_2]_2$ system; both M = Co and Fe showed metallic behavior above 15 and 35 K, respectively, as shown in Figure 30B. The magnetic susceptibility was again comparable to the TPP system (Figure 28B). The crystal with M = Co showed temperature-independent Pauli-like paramagnetism, while that with M = Fe showed large paramagnetism with a significant temperature dependence. Also, an anomaly indicating antiferromagnetic interactions was observed at around 20 K. Since the transport and magnetic properties are almost the same as those observed for the TPP system, the electronic structure in $[PTMA]_x[Fe(Pc)(CN)_2]\cdot y$(solvent) is expected to be the same as that in $TPP[Fe(Pc)(CN)_2]_2$. Indeed, the magnetoresistance measurements have revealed that $[PTMA]_x[M(Pc)(CN)_2]\cdot y$(solvent) also showed giant negative magnetoresistance at low temperature. The negative magnetoresistance is anisotropic again, and the details are described in section 4.4.

4.3. $M(Pc)(CN)_2$ Compounds with PXX

The open-shell π-radical cations were also subjected as the candidate of the cationic component for the partially oxidized $Co(Pc)(CN)_2$ salts. When electrolysis was done with relatively strong π-donors, the $[Co(Pc)(CN)_2]^-$ salt crystals in which only the π-donors were oxidized were obtained. For example, electrolysis with TTF gave a crystal of $[TTF][Co(Pc)(CN)_2]$.[91] The crystal structure is the same as that of $TPP[Co(Pc)(CN)_2]_2$, and one TPP cation is replaced by two TTF cation radicals. On the other hand, electrolysis with benzo[*c*]phenothiazine (B[*c*]PT) gave a 1:1 salt in which the B[*c*]PT cation radical was combined with a CN-bridged dimer unit of $Co(Pc)(CN)_2$, $[(CN)(Pc)Co-CN-Co(Pc)(CN)]^-$.[92] Finding this crystal proved that in solution the $[Co(Pc)(CN)_2]^-$ species exists as well as the dimerized species.

The above donors have a relatively small redox potential (0.2−0.5 V vs Ag/Ag^+), and the difference from that of the Pc ring (ca. 1 V) is rather large. Therefore, in the resultant crystals, only the donor components were oxidized. If one adopted PXX that is a π donor with a relatively large redox potential, partially oxidized salts in which both components were in partially oxidized states were obtained. This is interesting since this guide of "the difference of the redox potentials must be in some range" was proposed for the design of the conductors composed of a donor and an acceptor.[93,94] However, in contrast to the transport in the HOMO band of donors and LUMO band of acceptors in the donor−acceptor system, the partially filled bands in the $Co(Pc)(CN)_2$ system are composed of two kinds of HOMOs of each component.

Galvanostatic electrolysis of the acetonitrile solution containing $K[Co(Pc)(CN)_2]$ and PXX gave platelets and two kinds of needles. The needles are $[PXX][Co(Pc)(CN)_2]$ (PXX-1:1) and $[PXX]_2[Co(Pc)(CN)_2]$ (PXX-2:1), and the plate is $[PXX]_2[Co(Pc)(CN)_2]\cdot CH_3CN$. Among them, structural and physical properties were studied on the former two crystals.

It was important to determine the oxidation states of each component in these salts to know the electronic structure. Since it was difficult to obtain information on the oxidation state from the geometry or vibrational spectra of the Pc ring, the study was directed at PXX. The coefficients of the HOMO of PXX are concentrated at the central portion of the molecular framework, and systematic structural study of the PXX charge-transfer complexes revealed that the bond lengths at this portion varied depending on the formal charge of PXX.[95] From this relation the formal charge of PXX was found to be +0.5 in PXX-1:1, while it was found to be +0.25 in PXX-2:1. Therefore, the Pc ring is oxidized by 0.5e in both crystals.

The crystal of PXX-1:1 is composed of the 1D PXX columns with 2-fold periodicity and two-leg ladder chains of the $Co(Pc)(CN)_2$ units (Figure 33).[96] Both column and chain run parallel to the *c* axis. The neighboring Pc units along the *c* axis are related by a simple translation of the unit *c* length, and those in the rung of the ladder are related by an inversion center. Therefore, the ladder is constructed by two uniform equivalent chains. Though both components are oxidized by 0.5e in common, the overlap integrals are overwhelmingly larger between the Pc units than in the PXX column. Also, the PXX molecules are dimerized in the column. Therefore, charge transport exclusively occurs in the Pc ladder chain. The conductivity was 160 S cm^{-1} at room temperature and showed metallic behavior down to 100 K. This

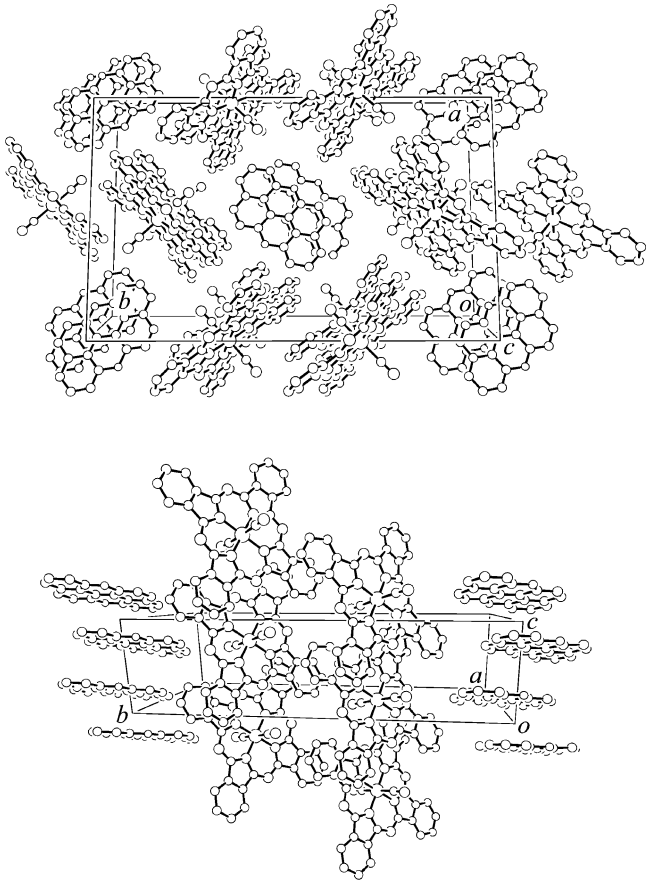

Figure 33. Crystal structure of [PXX][Co(Pc)(CN)$_2$] (PXX-1:1).

behavior is contrast to the vague metallic behavior in TPP[Co(Pc)(CN)$_2$]$_2$, though the overlap integral in this salt was nearly the same as that in PXX-1:1 along the chain direction. In the two-leg ladder chain, the conduction band consists of two overlapping 1D bands, and this difference in the electronic structure may be responsible for the clear metallic behavior in PXX-1:1.

The isomorphous crystal was obtained for the Fe(Pc)(CN)$_2$ unit.[97] In contrast to clear metallic conductivity above 100 K in PXX-1:1(Co), the temperature dependence of the conductivity in PXX-1:1(Fe) was entirely semiconducting with an activation energy of about 0.025 eV (Figure 31C). The room-temperature conductivity value was about one order of magnitude lower than that of PXX-1:1(Co), and the difference became very large at low temperature. The thermoelectric power of PXX-1:1(Co) showed clear metallic behavior down to 100 K. At lower temperature, the behavior changed to that indicating carrier localization.[97] The thermoelectric power of PXX-1:1(Fe) was also metallic above 100 K, though the temperature dependence of the conductivity was not metallic. The reflectance spectra also suggested that the electronic structure in PXX-1:1(Fe) is similar to that in PXX-1:1(Co); the spectra were practically the same. In both cases, the spectra were anisotropic and the plasma frequency observed polarization parallel to the chain direction suggested that the bandwidth along the leg was slightly smaller than that in the TPP salt, being consistent with the calculated overlap integral values.

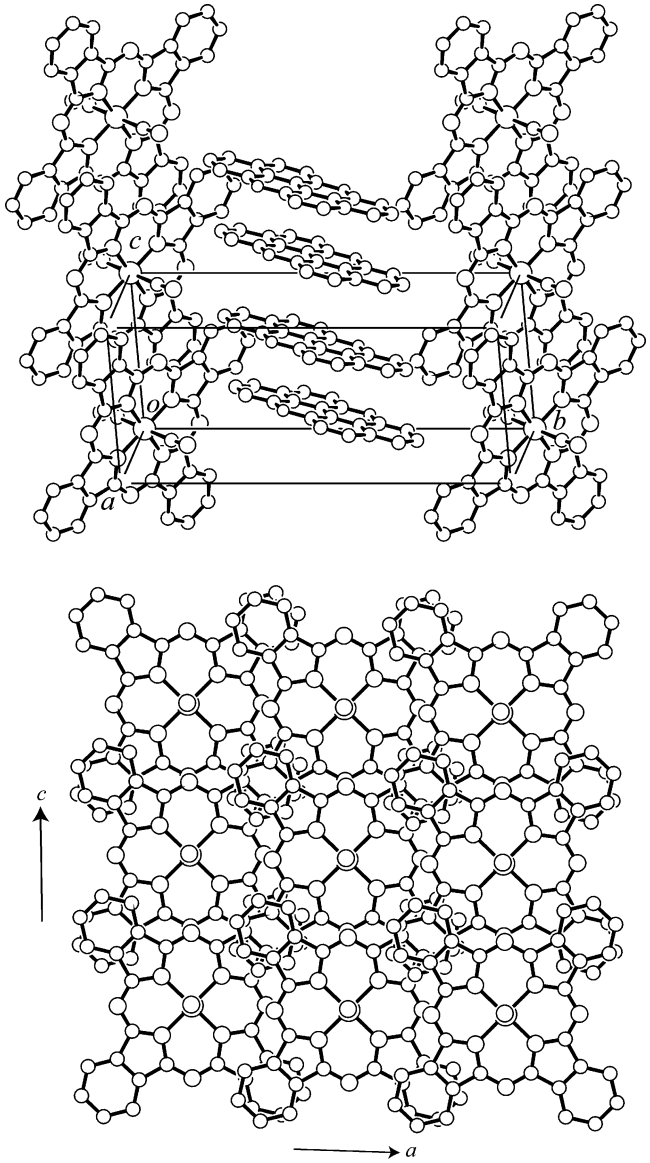

Figure 34. Crystal structure of [PXX]$_2$[Co(Pc)(CN)$_2$] (PXX-2:1).

The magnetic susceptibility of PXX-1:1(Fe) shows large paramagnetism with a significant temperature dependence. Similar to TPP[Fe(Pc)(CN)$_2$]$_2$ and [PTMA]$_x$[Fe(Pc)(CN)$_2$]·y(solvent), antiferromagnetic transition at low temperature was suggested. The magnetoresistance measurements were also performed for PXX-1:1(Fe) and revealed that the crystal showed giant negative magnetoresistance. The negative magnetoresistance was again largely anisotropic, and the relation between the anisotropy and the molecular arrangement is completely discussed in section 4.4 for TPP[Fe(Pc)(CN)$_2$]$_2$, [PTMA]$_x$[Fe(Pc)(CN)$_2$]·y(solvent), and PXX-1:1(Fe).

PXX-2:1 was a minor product contained in the crystals obtained by the electrolysis.[98] In this crystal, PXX forms a 1D column with 2-fold periodicity as in PXX-1:1 (Figure 34), but the dimerized structure is not so clear. The Co(Pc)(CN)$_2$ units are aligned along the c axis with type A overlaps between them and are connected infinitely along the [101] direction by type B overlaps (Figure 35). In both directions the neighboring molecules are related by a unit transla-

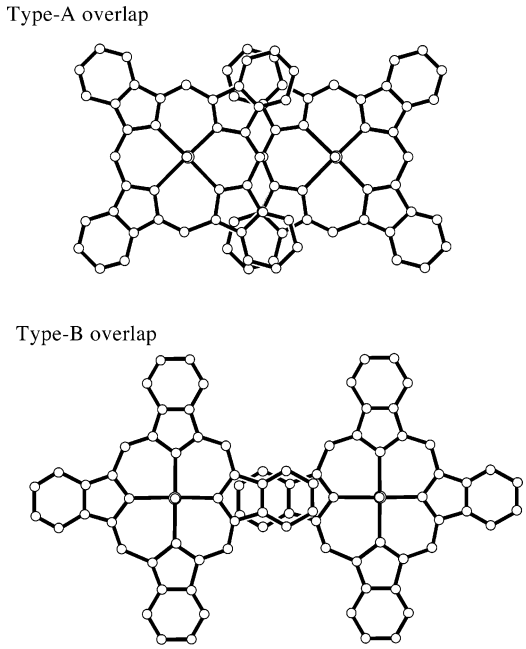

Figure 35. Two types of Pc ring overlaps.

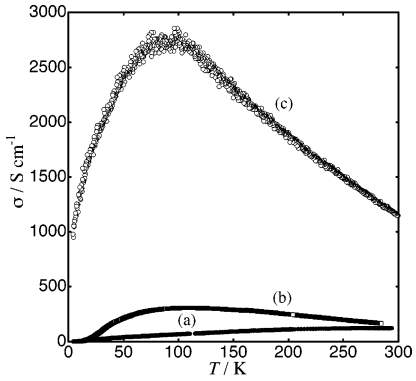

Figure 36. Temperature dependence of the electrical conductivity of (a) TPP[Co(Pc)(CN)$_2$]$_2$ (along the single Pc chain), (b) PXX-1:1(Co) (along the Pc ladder chain), and (c) PXX-2:1(Co) (along the *c* axis).

tion of the unit cell. Therefore, the total $\pi-\pi$-stacking structure becomes two-dimensional. However, due to the difference in the overlap integrals between type A and type B, the band calculation indicated that the conduction band was a modulated 1D band. The conductivity along the *c* axis was as high as 1000 S cm^{-1} at room temperature. The metallic behavior was observed down to 70 K, as shown in Figure 36c. The conductivity gradually decreased below this temperature, but even at 5 K it kept a high value of 1000 S cm^{-1}. The thermoelectric power was also metallic in the temperature range of 5−300 K. Since the PXX column has 2-fold periodicity, the bandwidth becomes narrow. Therefore, the PXX columns are supposed to negligibly contribute in the charge transport. The systematic comparison of the single-chain conductor of the TPP salt, the ladder chain conductor of PXX-1:1, and the 2D sheet conductor of PXX-2:1 in Figure 36 revealed that participation of the transverse $\pi-\pi$ interaction between the Pc stacking chains dramatically affects the transport properties, though some localization effects appeared at low temperature. The anisotropy of the electronic structure in the 2D sheet

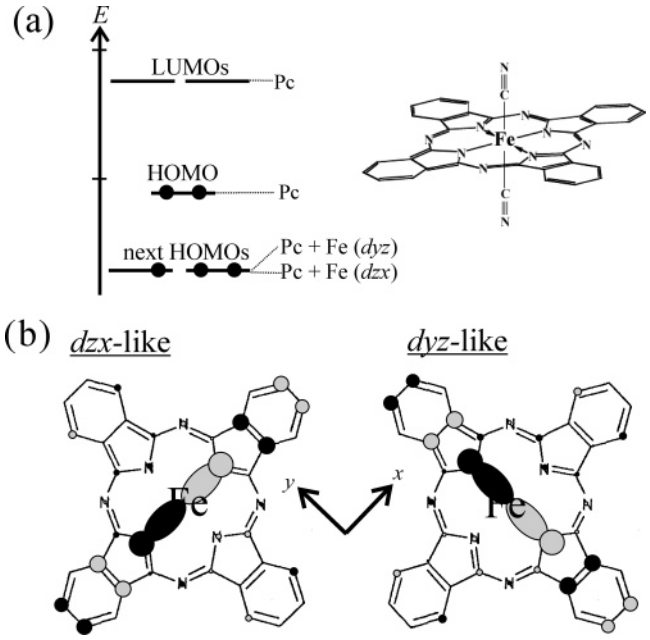

Figure 37. (a) Schematic energy diagram for [Fe(Pc)(CN)$_2$]$^-$; (b) symmetry of the next highest molecular orbitals.

in PXX-2:1 is still large, and indeed, the reflectance spectra showed a plasma edge only along the *c* axis.

4.4. π–d Interaction in the Fe(Pc)(CN)$_2$ System

[Fe(Pc)(CN)$_2$]$^-$ has a unique feature as a building block for molecular conductors. Figure 37a shows a schematic energy diagram obtained by use of a quantum chemical calculation (ZINDO).[85] In [M(Pc)(CN)$_2$]$^-$ (M = Co, Fe), HOMO is formed from the π orbital of the Pc ring, while the next HOMO's are degenerate d_{xy}- and d_{yz}-like orbitals (see Figure 37b). These orbitals are completely filled in [Co(Pc)(CN)$_2$]$^-$, while they are incompletely filled in [Fe(Pc)(CN)$_2$]$^-$. A conducting crystal is obtained by oxidation of [M(Pc)(CN)$_2$]$^-$. In the crystal, conduction carriers are the holes formed in the π orbital of the Pc ring. The degree of occupancy of the next HOMO is unaltered. Therefore, the unpaired electron in the next HOMOs in [Fe(Pc)(CN)$_2$]$^-$ works as a local magnetic moment. This is very similar to the case of the Cu(Pc) salts.

The most interesting feature of the Fe(Pc)(CN)$_2$ salt is that the unpaired electron is located in the degenerate d_{zx}- and d_{yz}-like orbitals. In this situation the degenerate energy levels split through the spin−orbit coupling (see Figure 38.) The resulting orbitals ($|1,\alpha\rangle$,$|-1,\beta\rangle$,$|-1,\alpha\rangle$,$|1,\beta\rangle$), have the orbital angular moment as well as the spin angular moment. As a consequence, large *g*-tensor anisotropy appears.[85] If we assume d_{zx} and d_{yz} instead of the next HOMOs and a positive spin−orbit coupling constant, $g \approx 4$ is expected for the field parallel to the CN axis and $g \approx 0$ for the field perpendicular to the CN axis. The estimates are very close to the *g* factors experimentally obtained in the ESR measurements of [PNP][Fe(Pc)(CN)$_2$] (see Figure 39, PNP = bis(triphenylphosphine)iminium).[85,99]

Figure 40 shows the temperature dependence of the resistivity for the three compounds of Fe(Pc)(CN)$_2$

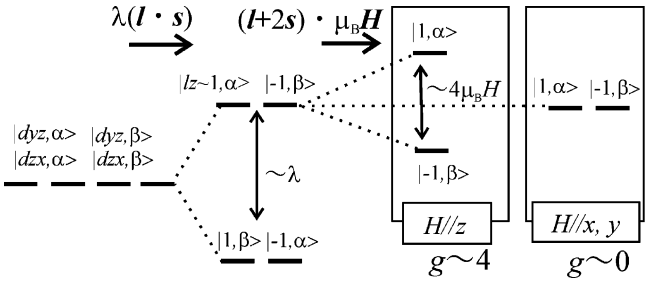

Figure 38. Illustrations for the explanation of the *g* tensor anisotropy in $[Fe(Pc)(CN)_2]^-$. The anisotropy arises from the orbital degeneracy of the next HOMOs through spin−orbit coupling.

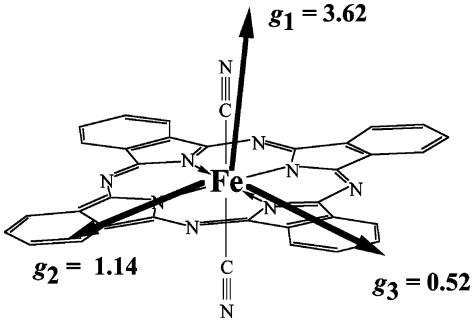

Figure 39. *g*-factor anisotropy experimentally determined by EPR for $PNP[Fe(Pc)(CN)_2]$. Due to the spin−spin coupling in the crystal, the 4-fold symmetry of the $[Fe(Pc)(CN)_2]^-$ unit is lost in the observed *g* factors.

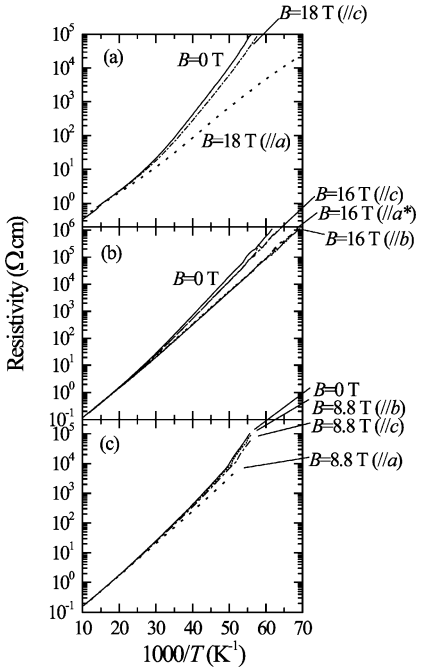

Figure 40. Temperature dependence of the resistivity of (a) $TPP[Fe(Pc)(CN)_2]_2$, (b) $[PXX][Fe(Pc)(CN)_2]$, and (c) $[PTMA]_x[Fe(Pc)CN]_2]\cdot y(CH_3CN)$ under the applied magnetic field.

in a magnetic field.[99] As can be seen from the figure, all these salts exhibit giant negative magnetoresistance. The negative magnetoresistance is highly anisotropic for the direction of the applied magnetic field. By taking the crystal structures shown in Figures 27, 32, and 33 into account, we see that the negative magnetoresistance tends to increase as the field direction approaches the direction of the CN axis. This trend is obvious in all three salts studied. Since the CN axis is approximately parallel to the g_1 direction in Figure 39, it is concluded that the *g* tensor anisotropy of the $Fe(Pc)(CN)_2$ unit rules the field-orientation dependence of the giant negative magnetoresistance in the $Fe(Pc)(CN)_2$ salts.

The $Fe(Pc)(CN)_2$ salts are similar to Cu(X)I (X = Pc, section 2.3; and X = tatbp, section 3.3) in a sense that conduction electrons and magnetic moments coexist in a system. Although all these salts exhibit peculiar magnetotransport properties, the negative magnetoresistance observed in $Fe(Pc)(CN)_2$ salts is somewhat different from the magnetotransport properties observed in Cu(X)I.

First, the negative magnetoresistance is highly anisotropic for the orientation of the applied magnetic field, reflecting the *g*-tensor anisotropy of the $Fe^{III}(Pc)(CN)_2$ unit. Such field-orientation dependence was not reported in Cu(X)I.

Second, the negative magnetoresistance of $TPP[Fe(Pc)(CN)_2]_2$ is larger than that of the alloys $TPP[Fe_xCu_{1-x}(Pc)(CN)_2]_2$.[89] Meanwhile, Cu(X)I does not exhibit negative magnetoresistance but the alloy $Cu_xNi_{1-x}(X)I$ does. According to Quirion et al.,[35] the absence of the negative magnetoresistance in Cu(Pc)I is due to the fact that the coupling of the local magnetic moments is too strong to be controlled by the applied magnetic field. This scenario does not seem to be applicable to $TPP[Fe(Pc)(CN)_2]_2$.

Third, $TPP[Co(Pc)(CN)_2]_2$, which does not have a local magnetic moment, exhibits large positive magnetoresistance. In the normal metal, the positive magnetoresistance arises from the Lorentz force affecting the mobile electrons. Therefore, positive magnetoresistance in the low-dimensional conductors is highly anisotropic for the magnetic-field orientation, reflecting the anisotropy of the Fermi velocity. On the other hand, such large anisotropy for the field orientation was not observed in the positive magnetoresistance of $TPP[Co(Pc)(CN)_2]_2$. Contrary to $TPP[Co(Pc)(CN)_2]_2$, the positive magnetoresistance in Ni(Pc)I seems to be the ordinary one expected in normal metals. Therefore, magnetoresistance phenomena in the $[Fe(Pc)(CN)_2]-[Co(Pc)(CN)_2]$ system are very different from those of the [Cu(Pc)]−[Ni(Pc)] system. More detailed studies are necessary to clarify the mechanism.

As described above, it is obvious that the giant negative magnetoresistance in $Fe(Pc)(CN)_2$ salts arises from the large d−π interaction within the $Fe(Pc)(CN)_2$ unit. However, the detailed mechanism of the giant negative magnetoresistance is still not understood well. The interest of this molecule for a component of molecular conductors is that the strong d−π interaction is promising in this molecule. This feature may be of use for fabricating molecular devices.

4.5. Other Partially Oxidized Salts

The axially Br-substituted $Co^{III}(Pc)Br_2$ unit also forms a partially oxidized salt with TPP. $TPP[Co(Pc)Br_2]_2$ is isomorphous with $TPP[Co(Pc)(CN)_2]_2$ and is a single chain 1D conductor.[86] The angularly π-extended Pc analogue with the C_{4h} point group, 1,2-

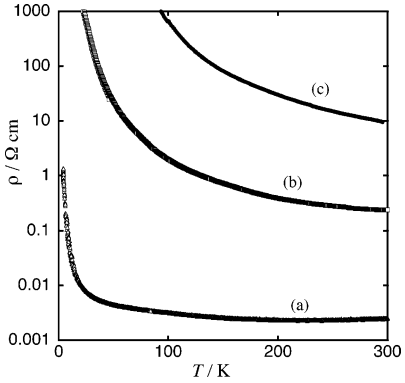

Figure 41. Temperature dependence of the electrical resistivity along the Pc (or 1,2-Nc) stacking direction in (a) TPP[Co(Pc)(CN)$_2$]$_2$, (b) TPP[Co(Pc)Br$_2$]$_2$, and (c) TPP[Co(1,2-Nc-C_{4h})(CN)$_2$]$_2$.

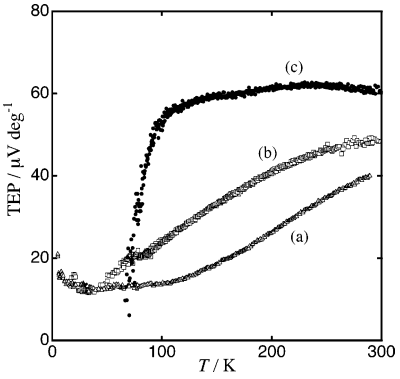

Figure 42. Temperature dependence of TEP along the Pc (or 1,2-Nc) stacking direction in (a) TPP[Co(Pc)(CN)$_2$]$_2$, (b) TPP[Co(Pc)Br$_2$]$_2$, and (c) TPP[Co(1,2-Nc-C_{4h})(CN)$_2$]$_2$.

naphthalocyanine (1,2-Nc-C_{4h}), was prepared, and the Co^{III}(1,2-Nc-C_{4h})(CN)$_2$ unit was found to form a partially oxidized salt of TPP[Co(1,2-Nc-C_{4h})(CN)$_2$]$_2$.[86] Though its complete structural analysis has not been reported yet, it was found that the crystal is a single chain 1D conductor with a tetragonal crystal system. In TPP[Co(Pc)(CN)$_2$]$_2$, TPP[Co(Pc)Br$_2$]$_2$, and TPP[Co(1,2-Nc-C_{4h})(CN)$_2$]$_2$, the oxidation state and the structural motif are in common. A comparison of the transport properties in these three salts is rather interesting, as shown in Figure 41. Though the metallic behavior was not clear in TPP[Co(Pc)(CN)$_2$]$_2$, it has a high conductivity at room temperature. The conductivity at room temperature in TPP[Co(Pc)Br$_2$]$_2$ is two orders lower than that in TPP[Co(Pc)(CN)$_2$]$_2$, and the temperature dependence becomes semiconducting. This less conducting tendency becomes more remarkable in TPP[Co(1,2-Nc-C_{4h})(CN)$_2$]$_2$; the room-temperature conductivity is more than three orders of magnitude lower than that in TPP[Co(Pc)(CN)$_2$]$_2$. This systematic change of the transport properties is related to the bandwidths in these salts. Compared with the CN group, Br is thicker and the $\pi-\pi$ overlap becomes less effective in TPP[Co(Pc)Br$_2$]$_2$. The angular π-extension of Pc also reduces the HOMO−HOMO overlap between the neighboring molecules due to the less effective overlap of the portions with large HOMO coefficients. These effects result in the systematic reduction of the bandwidth, and the correlation effect appears systematically. In fact, the thermoelectric power also varied systematically as shown in Figure 42; clear metallic behavior was observed in TPP[Co(Pc)(CN)$_2$]$_2$, while TEP of TPP[Co(1,2-Nc-C_{4h})(CN)$_2$]$_2$ showed a constant value of 60 μV deg^{-1} which is typical behavior for a strongly correlated 1D system with $\rho = 1/2$ (ρ is the number of charge carrier per one site).[100]

5. Neutral Radical Phthalocyanine Crystals

Though there are many studies about thin films of the neutral radical of Pc from an application viewpoint , only the studies on the single crystals are described in this review.

5.1. Li(Pc)

As there are various polymorphs of the plarnar M(Pc) system, three polymorphs of α, β, and x were reported for Li(Pc). Among them, high conductivity was reported only for x-Li(Pc), and this polymorph is described.

Li(Pc) was first obtained in 1978 by chemical oxidation.[101] Then electrochemical oxidation of Li$_2$(Pc) was found to give needle crystals of Li(Pc).[102] This needle corresponds to the x form, and the crystal structure resembles those of the M(Pc)X$_y$-type partially oxidized salt crystals; the crystal system is tetragonal with a space group *P4/nnc*. The staggering angle between the face-to-face overlapped molecules is 39°, and the Li···Li distance in the 1D column is 3.245 Å.

There have been several reports on the conductivity,[103−107] and the typical value is 10^{-3} S cm^{-1} at room temperature. The temperature dependence is semiconducting with an energy gap of 0.2 eV. From the reflectance spectra of the single crystal, on-site Coulomb energy $U = 1.5$ eV and transfer energy $t = 0.3$ eV were estimated.[22]

The magnetic susceptibility at room temperature was about 10% of the expected value for $S = 1/2$ noninteracting spins, and various temperature dependences were reported.[103,107−111] This system was known to show sample-dependent magnetic properties, and this specific property arose from its crystal structure. In the M(Pc)X$_y$-type partially oxidized salts, anions are aligned in a channel surrounded by the Pc columns arranged in the tetragonal lattice, while in Li(Pc), similar channels are formed between the Li(Pc) columns but they are empty. It was found that oxygen molecules could easily enter this channel, which significantly modified the ESR signal.[103] The intrinsic signal has a very narrow line width ($\Delta H_{1/2}$ = ca. 5 μT), but when the crystal is exposed to air, the line width increases more than 20 times. Furthermore, it was reported that the oxygen molecules connected the Li(Pc) radicals with ferromagnetic coupling.[110,112]

As a derivative, Li(Pc)I has been known. Though the compound has the same composition as M(Pc)I, it was not obtained by reaction of Li(Pc) with I$_2$ but was obtained by reaction between 1,2-dicyanobenzene and LiI.[108] The single-crystal X-ray structure analysis[113] revealed that the crystal was isomorphous with Ni(Pc)I. However, the Raman spectrum was different from that of Ni(Pc)I, and the iodide species was found

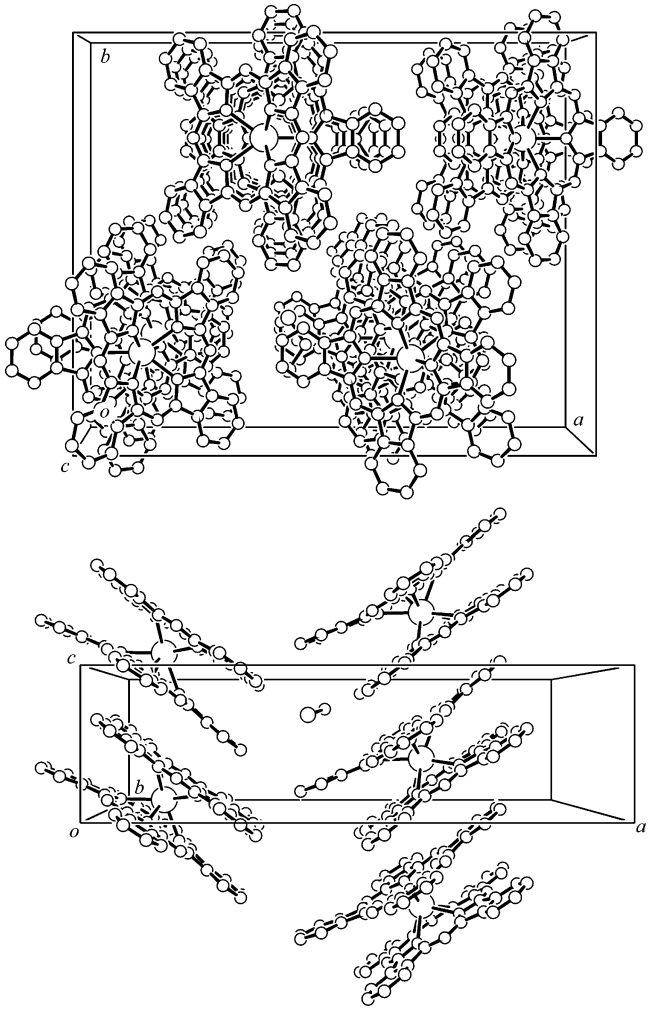

Figure 43. Crystal structure of $Lu(Pc)_2 \cdot CH_2Cl_2$.

to be different from I_3^-. The spacing between the Li-(Pc) molecules is 3.198 Å, and the staggering angle is almost 40°. Though the iodide species in this crystal has not become clear, the crystal is relatively conductive; the conductivity was 0.2 S cm^{-1} at room temperature, and the temperature dependence was semiconducting. The magnetic susceptibility was almost diamagnetic.[107]

5.2. $Ln(Pc)_2$

This system is famous for its electrochromism, and many studies have been done for the thin films. Though there have been some reports on the conductivity of the compressed pellets of the powders,[114−116] herein we describe only the results for the single crystals with clearly defined structures.

The most well-studied compound is $Lu(Pc)_2$, and two crystalline forms are known. In both crystals the sandwich-type radical molecule is the structural unit, but one form contains CH_2Cl_2 as the crystal solvent; the composition is $Lu(Pc)_2 \cdot CH_2Cl_2$. The other form is solvent-free $Lu(Pc)_2$. In $Lu(Pc)_2 \cdot CH_2Cl_2$, the radical molecules are arranged in a one-dimensional column as the β-form of M(Pc) (Figure 43).[117] On the other hand, in orthorhombic solvent-free $Lu(Pc)_2$, one radical molecule overlaps with four molecules and the dimensionality of the $\pi-\pi$-stacking network becomes

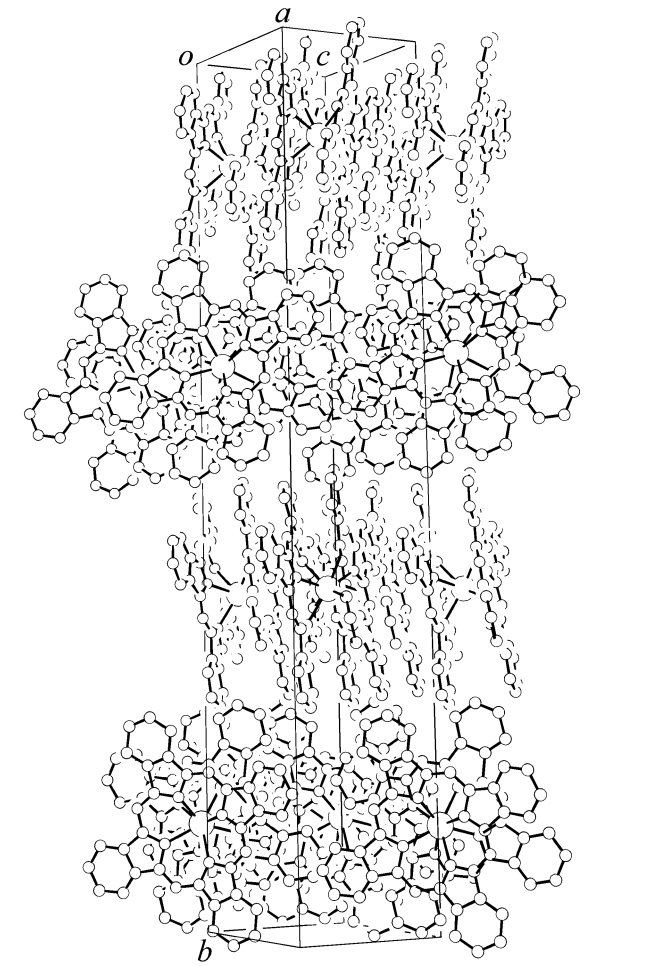

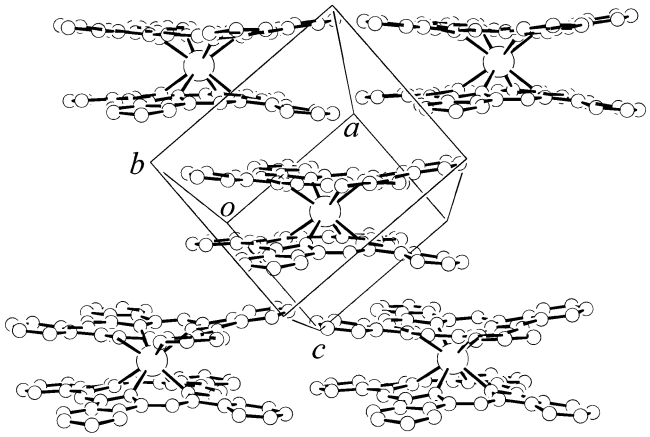

Figure 44. Crystal structure of $Lu(Pc)_2$.

two-dimensional (Figure 44).[118] These differences in the $\pi-\pi$ network dimensionality were confirmed by angular dependence measurements of the line width of the ESR signal.[119,120] The conductivity at room temperature was on the order of 10^{-5} S cm^{-1} in both crystals, and the bandwidths were suggested to be small.[119−121]

Li(Pc) and $Lu(Pc)_2$ were proposed as intrinsic molecular semiconductors,[122] and indeed, it was reported that their *p*- and *n*-doped semiconducting films were obtained by co-sublimation with acceptor molecules and with donor molecules, respectively.[123]

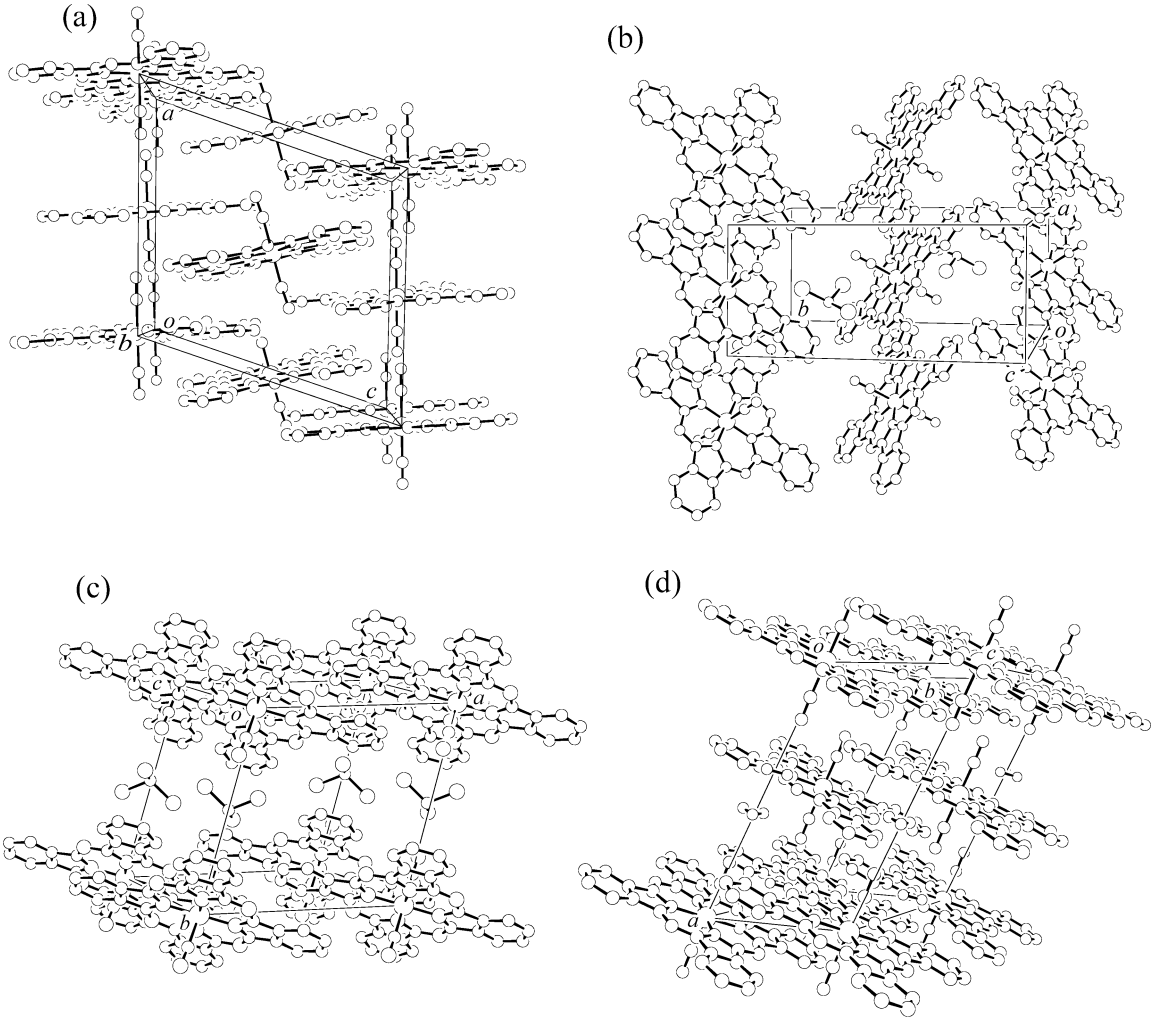

Figure 45. Crystal structures of the $Co(Pc)(CN)_2$ neutral radical: (a) solvent-free $Co(Pc)(CN)_2$, (b) $Co(Pc)(CN)_2 \cdot 2CHBr_3$, (c) $Co(Pc)(CN)_2 \cdot 2CHCl_3$, and (d) $Co(Pc)(CN)_2 \cdot 2H_2O$ (H_2O molecules are disordered).

5.3. $Co(Pc)(CN)_2$

As mentioned in section 4, electrochemical oxidation of the $[Co(Pc)(CN)_2]^-$ anion gave neutral radical crystals under some conditions. The most characteristic point of this compound is that it crystallizes with various crystal solvents and that various $\pi-\pi$-stacking structures arose from these solvent molecules. It is also possible to grow the solvent-free crystal, $Co(Pc)(CN)_2$.[124] In this case, the neighboring Pc rings are not parallel and the $\pi-\pi$ interactions are insufficient, as can be seen from Figure 45a. The conductivity was thus as low as 10^{-4} S cm^{-1} at room temperature. On the other hand, inclusion of crystal solvents makes the neighboring Pc planes parallel in the crystal, making the $\pi-\pi$ interactions more effective.

When the crystal solvent is $CHBr_3$, $Co(Pc)(CN)_2 \cdot 2CHBr_3$, 1D Pc arrangement as in $TPP[Co(Pc)(CN)_2]_2$ occurs (Figure 45b).[125] In this crystal, the Br atoms of $CHBr_3$ and the CN groups make short contacts. One $CHBr_3$ connects two $Co(Pc)(CN)_2$ units in neighboring chains. As a result, the Pc rings in these chains cannot be parallel to each other and the $\pi-\pi$-stacking network becomes 1D. The conductivity along the 1D chain at room temperature was 10^{-2} S cm^{-1}, which was two orders of magnitude higher than that of solvent-free crystal. The anisotropy of the conduction was found to be more than 10^2. The sign of TEP was negative, and TEP was found to linearly correlate with $1/T$. Therefore, the carriers are generated by thermal activation across the energy gap as in intrinsic semiconductors.[78] Since the chain is uniform, the origin of the gap is considered to be the on-site Coulomb repulsion energy.

When the crystal solvent is $CHCl_3$ or DMSO, 2D sheets of $Co(Pc)(CN)_2$ units, as in PXX-2:1, were found in the neutral radical crystals of $Co(Pc)(CN)_2 \cdot 2CHCl_3$ (Figure 45c)[126] and $Co(Pc)(CN)_2 \cdot 2DMSO$.[124] Each $CHCl_3$ forms a hydrogen bond with the CN group, but it is packed between the sheets without interfering with the formation of the 2D $\pi-\pi$-stacking structure. The DMSO molecules have no special contacts with the $Co(Pc)(CN)_2$ units and are packed as they compensate for the space formed between the sheets. The conductivity at room temperature was 10^{-1} S cm^{-1} along the sheet and 10^{-4} S cm^{-1} along the direction perpendicular to the sheet in both crystals. The TEP showed intrinsic semiconducting behavior as in $Co(Pc)(CN)_2 \cdot 2CHBr_3$.

When H_2O is the crystal solvent, the dimensionality of the $\pi-\pi$-stacking structure further increases.[76,126] 2D sheets are further closed as an extra $\pi-\pi$-stacking

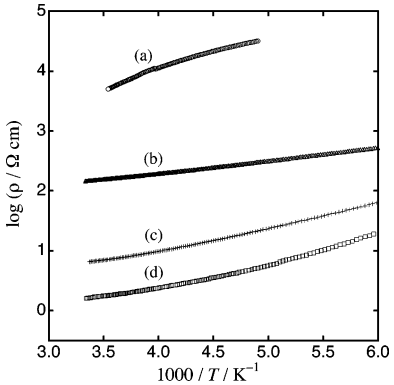

Figure 46. Temperature dependence of the resistivities of (a) $Co(Pc)(CN)_2$, (b) $Co(Pc)(CN)_2 \cdot 2CHBr_3$, (c) $Co(Pc)(CN)_2 \cdot 2CHCl_3$, and (d) $Co(Pc)(CN)_2 \cdot 2H_2O$.

interaction occurs between the sheets, and its total $\pi-\pi$-stacking network becomes three-dimensional (Figure 45d). The H_2O molecules occupy the small space in the network, and two H_2O molecules connect two CN groups in different $Co(Pc)(CN)_2$ units by hydrogen bonds. The interplanar spacing between these H_2O bridged two $Co(Pc)(CN)_2$ units is 14.173 Å. This spacing corresponds to the thickness of three Pc planes, and the 3D $\pi-\pi$-stacking network becomes possible. The conductivity at room temperature was 1 S cm^{-1}, and the anisotropy was also small.

In general, neutral radical crystals are poor conductors since carrier transport has to pay a cost for on-site Coulomb repulsion energy. However, the $Co(Pc)(CN)_2$ system shows rather high conductivity when the dimensionality of the $\pi-\pi$-stacking network becomes high, as shown in Figure 46. Though the metallic conductor has not been realized yet, it could be possible by applying pressure.

5.4. Other Neutral Radical Crystals

As a linearly π-extended Pc system, 2,3-naphthalocyanine (2,3-Nc) is known. By applying a crystal growth method similar to that of the $Co(Pc)(CN)_2$ system, the neutral radical crystals of $Co(2,3\text{-Nc})(CN)_2 \cdot CH_3CN$ and $Co(2,3\text{-Nc})(CN)_2 \cdot 2DCB$ (DCB = *o*-dichlorobenzene) were obtained.[127] The dimensionality of the $\pi-\pi$-stacking structure is increased compared to the Pc system owing to the extended π ring. The crystal included CH_3CN has a 3D $\pi-\pi$-stacking network, and the conductivity at room temperature is 0.3 S cm^{-1} with an activation energy of 0.11 eV. Though DCB is considerably larger than the solvent molecules in the Pc system, the crystal of $Co(2,3\text{-Nc})(CN)_2 \cdot 2DCB$ maintains the 2D $\pi-\pi$-stacking network. Unfortunately, the crystal was unstable, and no data on the charge-transport properties has been reported.

By electrolysis of Zn(Pc) with a chloride electrolyte, neutral radical crystals of Zn(Pc)Cl were obtained in which the Pc ring was oxidized.[128,129] The five-coordinate Zn atom is extruded from the Pc ring by 0.59 Å. The crystal system is tetragonal, and two Zn(Pc)Cl units form a dimer unit with the planar parts facing each other (Figure 47; interplanar spacing, 3.16 Å; staggering angle, 39°). In the crystal, this dimer unit has $\pi-\pi$ contacts with eight dimer units

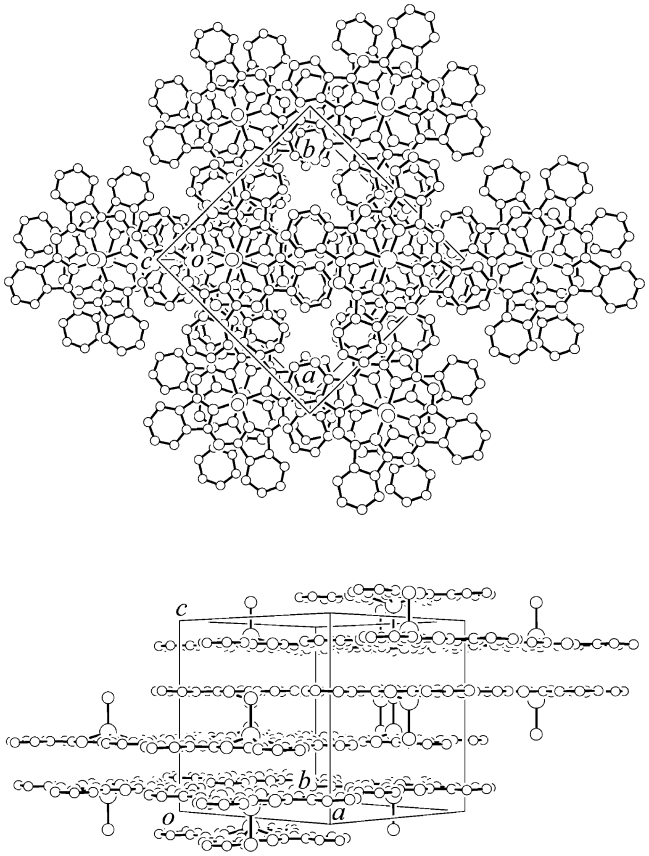

Figure 47. Crystal structure of Zn(Pc)Cl.

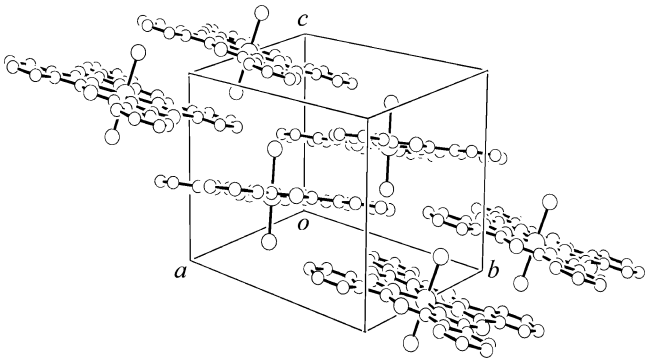

Figure 48. Crystal structure of $Cr(Pc)Cl_2$.

with an interplanar spacing of 3.38 Å, and the total $\pi-\pi$ interaction becomes 3D. The conductivity at room temperature is 10^{-1} S cm^{-1}. This crystal is a semiconductor with an energy gap of 0.16 eV.

The similar electrolysis of Cr(Pc), Fe(Pc), and Co(Pc) was reported to give neutral radical crystals of $Cr(Pc)Cl_2$, $Fe(Pc)Cl_2$, and $Co(Pc)Cl_2$, respectively.[130] They are all isomorphous with a monoclinic crystal system. As shown in Figure 48, the $\pi-\pi$ network is 1D, and the conductivity is in a range of $10^{-3}-10^{-2}$ S cm^{-1} at room temperature. The activation energy is about 0.13 eV.

When the Cr powder was reacted with 1,2-dicyanobenzene under coexistence of I_2 vapor, neutral radical crystals of $Cr(Pc)I_2 \cdot I_2$ were obtained.[131] In the crystal, two I^- anions are axially coordinated to Cr(Pc), forming the $Cr(Pc)I_2$ unit. These units are bridged by neutral I_2 molecules and form an infinite zigzag chain. There are appreciable $\pi-\pi$ overlaps

between the chains (interplanar spacing of 3.258 Å). The conductivity at room temperature of the pressed pellet was 10^{-2} S cm^{-1}. Strangely, the temperature dependence was not thermally activated down to 15 K; a rather weak metal-like behavior was reported.

6. Conclusion

In this review Pc-based conductors with clearly defined structures have been described. As shown in section 2, when planar Pc complexes were the components, only the 1D system was obtained. However, these studies revealed that they had rather unique properties as a 1D system. Also, it was found that the electronic properties at low temperature were severely affected by the defects or impurities in the crystal due to their highly one-dimensional electronic structure. As a result, it has become clear that most of the M(Pc)X_y one-dimensional partially oxidized salts do not show metal-to-insulator transitions with definite lattice distortions down to very low temperature. The next step may be to elucidate the ground state of these substances.

Metal−phthalocyanines are relatively flexible to chemical modification, and by using this feature versatility as a component of molecular conductors has been realized. One is the axial ligand coordination of the central metal, and axially substituted Pc compounds mentioned in sections 4 and 5 have developed various $\pi-\pi$-stacking structures, in contrast to the preferential metal-over-metal stacking structures in planar M(Pc) conductors. This structural variation of the $\pi-\pi$-stacking dimensionality is expected to produce still more various novel conductors in the future, possibly extending to novel superconductors.

The other is metal substitution, and this has made it possible to design molecular conductors introducing magnetic moments in the center of the π system. In either the planar M(Pc)X_y system or the axially substituted M(Pc)$(CN)_2$ system, this modification generated modulation in the conduction electron systems, and peculiar properties such as giant negative magnetoresistance have appeared.

Furthermore, it is possible to modify the Pc ring itself. Since the substitutions of π-extended Nc and porphyrinic ligands will lead to changes in not only the shape but also the energy levels and orbital coefficients of HOMO, further various physical properties are expected to be realized by proper design of the π-ligand in addition to regulation of the $\pi-\pi$-stacking structure.

7. Abbreviations Used

Pc	phthalocyaninato
tatbp	triazatetrabenzoporphyrinato
tbp	tetrabenzoporphyrinato
tmp	tetramethylporphyrinato
TPP	tetraphenylphosphonium
PTMA	phenyltrimethylammonium
PXX	*peri*-xanthenoxanthene (6,12-dioxaanthanthrene in IUPAC)

8. Acknowledgments

The work cited in sections 4 and 5.3 was supported in part by a Grant-in Aid for Scientific Research on Priority Areas of Molecular Conductors (15073207 and 15073101) from the Ministry of Education, Culture, Sports, Science and Technology of the Japanese Government and a Grant-in Aid for Scientific Research (A) (15205018) of Japan Society for the Promotion of Science. The authors are grateful to Drs. Noriaki Hanasaki and Masaki Matsuda for their collaboration.

9. References

(1) *Phthalocyanines: Properties and Applications*; Leznoff, C. C., Lever, A. B. P., Eds.; Wiley-VCH: Cambridge, 1989−1996; Vols. 1−4.
(2) Marks, T. J. *Angew. Chem., Int. Ed. Engl*. **1990**, *29*, 857.
(3) Hanack, M.; Lang, M. *Adv. Mater*. **1994**, *6*, 819.
(4) Hanack, M.; Datz, A.; Fay, R.; Fischer, K.; Keppeler, U.; Koch, J.; Metz, J. Mezger, M.; Schneider, O.; Schulze, H.-J. *Handbook of Conducting Polymers*; Skotheim, T. A., Ed.; Marcel Dekker: New York, 1986.
(5) Thompson, J. A.; Murata, K.; Miller, D. C.; Stanton, J. L.; Broderick, W. E.; Hoffman, B. M.; Ibers, J. A. *Inorg. Chem*. **1993**, *32*, 3546.
(6) Yakushi, K.; Simonyan, M.; Ding, Y. *J. Porphyrins Phthalocyanines* **2001**, *5*, 13.
(7) Petersen, J. L.; Schramm, C. S.; Stojakovic, D. R.; Hoffman, B. M.; Marks, T. J. *J. Am. Chem. Soc*. **1977**, *99*, 286.
(8) Schramm, C. S.; Scaringe, R. P.; Stojakovic, D. R.; Hoffman, B. M.; Ibers, J. A.; Marks, T. J. *J. Am. Chem. Soc*. **1980**, *102*, 6702.
(9) Martinsen, J.; Palmer, S. M.; Tanaka, J.; Greene, R.; Hoffman, B. M. *Phys. Rev. B* **1984**, *30*, 6269.
(10) Diel, B. N.; Inabe, T.; Lyding, J. W.; Schoch, K. F., Jr.; Kannewurf, C. R.; Marks, T. J. *J. Am. Chem. Soc*. **1983**, *105*, 1551.
(11) Murata, K.; Ohashi, Y.; Murata, K.; Thompson, J. A.; Mori, M.; Hoffman, B. M. *Synth. Met*. **1993**, *56*, 1777.
(12) Palamer, S. M.; Stanton, J. L.; Hoffman, B. M.; Ibers, J. A. *Inorg. Chem*. **1986**, *25*, 2296.
(13) Inabe, T.; Nakamura, S.; Liang, W.-B.; Marks, T.; Burton, R. L.; Kannewurf, C. R.; Imaeda, K. *J. Am. Chem. Soc*. **1985**, *107*, 7724.
(14) Almeida, M.; Kanatzidis, M. G.; Tonge, L. M.; Marks, T. J.; Marcy, H. O.; McCarthy, W. J.; Kannewurf, C. R. *Solid State Commun*. **1987**, *63*, 457.
(15) Yakushi, K.; Sakuda, M.; Kuroda, H.; Kawamoto, A.; Tanaka, J. *Chem. Lett.* **1986**, 1161.
(16) Yakushi, K.; Yamakado, H.; Yoshitake, A.; Kosugi, N.; Kuroda, H.; Sugano, T.; Kinoshita, M.; Kawamoto, A.; Tanaka, J. *Bull. Chem. Soc. Jpn*. **1989**, *62*, 687.
(17) Yakushi, K.; Sakuda, M.; Hamada, I.; Kuroda, H.; Kawamoto, A.; Tanaka, J.; Sugano, T.; Kinoshita, M. *Synth. Met.* **1987**, *19*, 769.
(18) Yamakado, H.; Ugawa, A.; Ida, T.; Yakushi, K. *The Physics and Chemistry of Organic Superconductors*; Saito, G., Kagoshima, S., Eds.; Springer-Verlag: New York, 1989; pp 311−314.
(19) Yakushi, K.; Hiejima, T.; Yamakado, H. *Materials and Measurements in Molecular Electronics*; Kajimura, K., Kuroda, S., Eds.; Springer-Verlag: New York, 1996; pp 203−216.
(20) Ida, T.; Yamakado, H.; Masuda, H.; Yakushi, K. *Mol. Cryst. Liq. Cryst.* **1990**, *181*, 243.
(21) Yakushi, K.; Yamakado, H.; Ida, T.; Ugawa, A. *Solid State Commun.* **1991**, *78*, 919.
(22) Yakushi, K.; Ida, T.; Ugawa, A.; Yamakado, H.; Ishii, H.; Kuroda, H. *J. Phys. Chem.* **1991**, *95*, 7636.
(23) Hiejima, T.; Yakushi, K. *J. Chem. Phys.* **1995**, *103*, 3950.
(24) Toman, P.; Nespurek, S.; Yakushi, K. *J. Porphyrins Phthalocyanines* **2002**, *6*, 556.
(25) Hiejima, T.; Yakushi, K.; Adachi, T.; Shimomura, O.; Takeda, K.; Shirotani, I.; Imaeda, K.; Inokuchi, H. *Mol. Cryst. Liq. Cryst.* **1997**, *296*, 255.
(26) Yonehara, Y.; Yakushi, K. *Synth. Met.* **1998**, *94*, 149.
(27) Inabe, T.; Marks, T. J.; Burton, R. L.; Lyding, J. W.; McCarthy, W. J.; Kannewurf, C. R.; Reisner, G. M.; Herbstein, F. H. *Solid State Chem*. **1985**, 54, *501*.
(28) Lee, Y.; Harvey, H.; Haard, T. M.; Hamot, P. J.; Halperin, W. P.; Thompson, J. A.; Hoffman, B. M. *Physica B* **1994**, *194−196*, 1263.
(29) Liou, K.; Newcomb, T. P.; Heagy, M. D.; Thompson, J. A.; Heuer, W. B.; Musselman, R. L.; Jacobsen, C. S.; Hoffman, B. M.; Ibers, J. A. *Inorg. Chem*. **1992**, *31*, 4517.
(30) Ogawa, M. Y.; Martinsen, J.; Palmer, S. M.; Stanton, J. L.; Tanaka, J.; Greene, R. L.; Hoffman, B. M.; Ibers, J. A. *J. Am. Chem. Soc.* **1987**, *109*, 1115.
(31) Ogawa, M. Y.; Hoffman, B. M.; Lee, S.; Yudkowsky, M.; Halperin, W. P. *Phys. Rev. Lett.* **1986**, *57*, 1177.

(32) Ogawa, M. Y.; Palmer, S. M.; Liou, K K.; Quirion, G.; Thompson, J. A.; Poirier, M.; Hoffman, B. M. *Phys. Rev. B* **1989**, *39*, 10682.
(33) Quirion, G.; Poirier, M.; Ayache, C.; Liou, K. K.; Hoffman, B. M. *J. Phys. I Fr.* **1992**, *2*, 741.
(34) Rende, D. E.; Heagy, M. D.; Heuer, W. B.; Liou, K.; Thompson, J. A.; Hoffman, B. M.; Musselman, R. L. *Inorg. Chem.* **1992**, *31*, 352.
(35) Quirion, G.; Poirier, M.; Liou, K. K.; Hoffman, B. M. *Phys. Rev. B* **1991**, *43*, 860.
(36) Thompson, J. A.; Murata, K.; Durcharne, R.; Poirier, M.; Hoffman, B. M. *Phys. Rev. B* **1999**, *60*, 523.
(37) Martin, I.; Phillip, P. *Phys. Rev. B* **1999**, *60*, 530.
(38) Martinsen, J.; Stanton, J. L.; Greene, R. L.; Tanaka, J.; Hoffman, B. M.; Ibers, J. A. *J. Am. Chem. Soc.* **1985**, *107*, 6915.
(39) Quirion, G.; Poirier, M.; Castonguay, M.; Liou, K. K.; Hoffman, B. M. *Phys. Rev. B* **1990**, *42*, 2831.
(40) Liou, K.; Jacobsen, C. S.; Hoffman, B. M. *J. Am. Chem. Soc.* **1989**, *111*, 6616.
(41) Yamakado, H.; Ida, T.; Ugawa, A.; Yakushi, K.; Awaga, K.; Maruyama, Y.; Imaeda, K.; Inokuchi, H. *Synth. Met*. **1994**, *62*, 169.
(42) Ding, Y.; Simonyan, M.; Yonehara, Y.; Uruichi, M.; Yakushi, K. *J. Mater. Chem.* **2001**, *11*, 1469.
(43) Yakushi, K.; Yamakado, H.; Ida, T.; Ugawa, A.; Awaga, K.; Maruyama, Y.; Imaeda, K.; Inokuuchi, H. *Synth. Met.* **1993**, *56*, 1699.
(44) Simonyan, M.; Yonehara, Y.; Ding, Y.; Yakushi, K. *Phys. Rev. B* **2001**, *63*, 113103.
(45) Yamakado, H.; Yakushi, K.; Kosugi, N.; Kuroda, H.; Kawamoto, A.; Tanaka, J.; Sugano, T.; Kinoshita, M.; Hino, S. *Bull. Chem. Soc. Jpn.* **1989**, *62*, 2267.
(46) Hino, S.; Matsumoto, K.; Yamakado, H.; Yakushi, K.; Kuroda, H. *Synth. Met.* **1989**, *32*, 301.
(47) Palamer, S. M.; Stanton, J. L.; Jaggi, N. K.; Hoffman, B. M.; Ibers, J. A.; Schwartz, L. H. *Inorg. Chem*. **1985**, *24*, 2040.
(48) Janczak, J.; Kubiak, R.; Hahn, F. *Inorg. Chim. Acta* **1998**, *281*, 195.
(49) Janczak, J.; Kubiak, R.; Jezierski, A. *Inorg. Chem*. **1999**, *38*, 2043.
(50) Janczak, J.; Idemori, Y. M. *Inorg. Chim. Acta* **2001**, *325*, 85.
(51) Capobianchi, A.; Ercolani, C.; Paoletti, A. M.; Pennesi, G.; Rossi, G.; Chiesi-Villa, A.; Rizzoli, C. *Inorg. Chem*. **1993**, *32*, 4605.
(52) Janczak, J.; Kubiak, R. *Polyhedron* **1999**, *18*, 1621.
(53) Janczak, J.; Kubiak, R.; Svoboda, I.; Jezierski, A.; Fuess, H. *Inorg. Chim. Acta* **2000**, *304*, 150.
(54) Martinsen, J.; Pace, L. J.; Phillips T. E.; Hoffman, B. M.; Ibers, J. A. *J. Am. Chem. Soc*. **1982**, *104*, 83.
(55) Murata, K.; Liou, K.; Thompson, J. A.; McGhee, E. M.; Rende, D. E.; Ellis, D. E.; Musselman, R. L.; Hoffman, B. M.; Ibers, J. A. *Inorg. Chem*. **1997**, *36*, 3363.
(56) Euler, W. B.; Martinsen, J.; Pace, L. J.; Hoffman, B. M.; Ibers, J. A. *Mol. Cryst. Liq. Cryst*. **1982**, *81*, 231.
(57) Hoffman, B. M.; Ibers, J. A. *Acc. Chem. Res*. **1983**, *16*, 15.
(58) Palamer, S. M.; Stanton, J. L.; Martinsen, J.; Ogawa, M. Y.; Heuer, W. B.; Van Wallendeal, S. E.; Hoffman, B. M.; Ibers, J. A. *Mol. Cryst. Liq. Cryst*. **1985**, *125*, 1.
(59) Pace, L. J.; Martinsen, J.; Ulman, A.; Hoffman, B. M.; Ibers, J. A. *J. Am. Chem. Soc*. **1983**, *105*, 2612.
(60) Newcomb, T. P.; Godfrey, M. R.; Hoffman, B. M.; Ibers, J. A. *J. Am. Chem. Soc*. **1989**, *111*, 7078.
(61) Newcomb, T. P.; Godfrey, M. R.; Hoffman, B. M.; Ibers, J. A. *Inorg. Chem*. **1990**, *29*, 223.
(62) Pietro, W. J.; Marks, T. J.; Ratner, M. A. *J. Am. Chem. Soc*. **1985**, *107*, 5387.
(63) Liou, K.; Ogawa, M. Y.; Newcomb, T. P.; Quirion, G.; Lee, M.; Poirier, M.; Halperin, W. P.; Hoffman, B. M.; Ibers, J. A. *Inorg. Chem.* **1989**, *28*, 3889.
(64) Quirion, G.; Poirier, M.; Liou, K. K.; Ogawa, M. Y.; Hoffman, B. M. *Phys. Rev. B* **1988**, *37*, 4272.
(65) McGhee, E. M.; Godfrey, M. R.; Hoffman, B. M.; Ibers, J. A. *Inorg. Chem*. **1991**, *30*, 803.
(66) McGhee, E. M.; Hoffman, B. M.; Ibers, J. A. *Inorg. Chem*. **1991**, *30*, 2162.
(67) Phillips, T. E.; Hoffman, B. M. *J. Am. Chem. Soc*. **1977**, *99*, 7734.
(68) Phillips, T. E.; Scaringe, R. P.; Hoffman, B. M.; Ibers, J. A. *J. Am. Chem. Soc*. **1980**, *102*, 3435.
(69) Godfrey, M. R.; Newcomb, T. P.; Hoffman, B. M.; Ibers, J. A. *J. Am. Chem. Soc*. **1990**, *112*, 7260.
(70) Yakushi, K.; Yoshitake, M.; Kuroda, H.; Kawamoto, A.; Tanaka, J.; Sugano, T.; Kinoshita, M. *Bull. Chem. Soc. Jpn*. **1988**, *61*, 1571.
(71) Metz, J.; Hanack, M. *J. Am. Chem. Soc*. **1983**, *105*, 828.
(72) Orihashi, Y.; Kobayashi, N.; Tsuchida, E.; Matsuda, H.; Nakanishi, H.; Kato, M. *Chem. Lett*. **1985**, 1617.
(73) Orihashi, Y.; Kobayashi, N.; Ohno, H.; Tsuchida, E.; Matsuda, H.; Nakanishi, H.; Kato, M. *Synth. Met*. **1987**, *19*, 751.
(74) Orihashi, Y.; Kobayashi, N.; Ohno, H.; Tsuchida, E.; Matsuda, H.; Nakanishi, H.; Kato, M. *Mol. Cryst. Liq. Cryst*. **1988**, *160*, 139.
(75) Inabe, T.; Maruyama, Y. *Chem. Lett*. **1989**, 55.
(76) Inabe, T.; Maruyama, Y. *Bull. Chem. Soc. Jpn*. **1990**, *63*, 2273.
(77) Inabe, T.; Maruyama, Y.; Mitsuhashi, T. *Synth. Met.* **1991**, *41*−*43*, 2629.
(78) Inabe, T. *J. Porphyrins Phthalocyanines* **2001**, *5*, 3.
(79) Hasegawa, H.; Naito, T.; Inabe, T.; Akutagawa, T.; Nakamura, T. *J. Mater. Chem*. **1998**, *8*, 1567.
(80) Dance, I.; Scudder, M. *J. Chem. Soc., Dalton Trans*. **1996**, 3755.
(81) Matsuda, M.; Naito, T.; Inabe, T.; Hanasaki, N.; Tajima, H.; Otsuka, T.; Awaga, K.; Narymbetov, B.; Kobayashi, H. *J. Mater. Chem*. **2000**, *10*, 631.
(82) Hanasaki, N.; Tajima, H.; Matsuda, M.; Naito, T.; Inabe, T. *Phys. Rev. B* **2000**, *62*, 5839.
(83) Matsuda, M.; Hanasaki, N.; Tajima, H.; Sakai, F.; Naito, T.; Inabe, T. *Synth. Met.* **2003**, *135*, 635.
(84) Hanasaki, N.; Matsuda, M.; Tajima, H.; Naito, T.; Inabe, T. *Synth. Met.* **2003**, *137*, 1227.
(85) Hanasaki, N.; Matsuda, M.; Tajima, H.; Naito, T.; Inabe, T. *J. Phys. Soc. Jpn.* **2003**, *72*, 3226.
(86) Inabe, T.; Asari, T.; Hasegawa, H.; Matsuda, M.; Gacho, E. H.; Matsumura, N.; Takeda, K.; Naito, T. *Synth. Met*. **2003**, *133*−*134*, 515.
(87) Hanasaki, N.; Matsuda, M.; Tajima, H.; Ohmichi, E.; Osada, T.; Naito, T.; Inabe, T. Submitted for publication.
(88) For example, see: Advances in Synthetic Metals; Bernier, P., Lefrant, S., Bidan, G., Eds.; Elsevier Science: New York, 1999.
(89) Tajima, H.; Hanasaki, N.; Matsuda, M.; Sakai, F.; Naito, T.; Inabe, T. *J. Solid State Chem.* **2002**, *168*, 509.
(90) Matsuda, M.; Naito, T.; Inabe, T.; Hanasaki, N.; Tajima, H. *J. Mater. Chem*. **2001**, *11*, 2493.
(91) Hasegawa, H.; Takano, S.; Miyajima, N.; Inabe, T. *Mol. Cryst. Liq. Cryst*. **1996**, *285*, 113.
(92) Takano, S.; Naito, T.; Inabe, T. *J. Mater. Chem*. **1998**, *8*, 511.
(93) Saito, G.; Ferraris, J. P. *Bull. Chem. Soc. Jpn.* **1980**, *53*, 2141.
(94) Torrance, J. B. *Acc. Chem. Res*. **1979**, *12*, 79.
(95) Asari, T.; Kobayashi, N.; Naito, T.; Inabe, T. *Bull. Chem. Soc. Jpn*. **2001**, *74*, 53.
(96) Takano, S.; Naito, T.; Inabe, T. *Chem. Lett*. **1998**, 1249.
(97) Matsuda, M.; Asari, T.; Naito, T.; Inabe, T.; Hanasaki, N.; Tajima, H. *Bull. Chem. Soc. Jpn*. **2003**, *76*, 1935.
(98) Asari, T.; Naito, T.; Inabe, T.; Matsuda, M.; Tajima, H. *Chem. Lett*. **2004**, *33*, 128.
(99) Matsuda, M.; Hanasaki, N.; Tajima, H.; Naito, T.; Inabe, T. *J. Phys. Chem. Solids* **2004**, *65*, 749.
(100) Chaikin, P. M.; Beni, G. *Phys. Rev. B* **1976**, 13, 647.
(101) Homborg, H.; Kalz, W. *Z. Naturforsch., B: Anorg. Chem. Org. Chem.* **1978**, *33B*, 1067.
(102) Sugimoto, H.; Higashi, T.; Mori, M. *J. Chem. Soc., Chem. Commun*. **1983**, 622.
(103) Turek, P.; Andre, J. J.; Simon, J. *Solid State Commun.* **1987**, *63*, 741.
(104) Turek, P.; Moussavi, M.; Petit, P.; Andre, J. J. *Synth. Met*. **1989**, *29*, F65.
(105) Dumm, M.; Lunkenheimaer, P.; Loidl, A.; Assmann, B.; Homborg, H.; Fulde, P. *J. Chem. Phys*. **1996**, *104*, 5048.
(106) Dumm, M.; Spitzfaden, R.; Lunkenheimer, P.; Dressel, M.; Loidl, A.; Assmann, B.; Homborg, H.; Fulde, P. *Synth. Met*. **1997**, *84*, 925.
(107) Dumm, M.; Dressel, M.; Nicklas, M.; Lunkenheimer, P.; Loidl, A.; Weiden, M.; Steglich, F.; Assmann, B.; Homborg, H.; Fulde, P. *Euro. Phys. J., B: Condens. Matter Phys.* **1998**, *6*, 317.
(108) Homborg, H.; Teske, C. L. *Z. Anorg. Allg. Chem*. **1985**, *527*, 45.
(109) Sugimoto, H.; Mori, M.; Masuda, H.; Taga, T. *J. Chem. Soc., Chem. Commun*. **1986**, 962.
(110) Turek, P.; Moussavi, M.; Andre, J. J. *Europhys. Lett.* **1989**, *8*, 275.
(111) Brinkmann, M.; Turek, P.; Andre, J. J. *J. Mater. Chem*. **1998**, *8*, 675.
(112) Turek, P.; Moussavi, M.; Andre, J. J.; Fillion, G. *J. Phys., Colloque* **1988**, *C8*, 835.
(113) Latte, A.; Kienast, A.; Bruhn, C.; Loidl, A.; Homborg, H. *J. Porphyrin Phthalocyanine* **1997**, *1*, 267.
(114) Yamana, M.; Tsutsui, M.; Ham, J. S. *J. Chem. Phys*. **1982**, *76*, 2761.
(115) Sullivan, B. W.; Dominey, R. N.; Helms, J, H.; Schwartz, M.; ter Haar, L. W.; Hatfield, W. E. *Mol. Cryst. Liq. Cryst*. **1985**, *120*, 433.
(116) Padilla, J.; Hatfield, W. E. *Inorg. Chim. Acta* **1991**, *185*, 131.
(117) De Cian, A.; Moussavi, M.; Fischer, J.; Weiss, R. *Inorg. Chem*. **1985**, *24*, 3162.
(118) Darouskikh, A. N.; Frank-Kamentskaya, O. V.; Fundamenskii, V. S.; Golubev, A. M. *Krystallografiya* **1986**, *31*, 455.
(119) Pitet, P.; Holczer, K.; Andre, J.-J. *J. Phys.* **1987**, *48*, 1363.
(120) Petit, P.; Andre, J.-J. *J. Phys. Fr.* **1988**, *49*, 2059.
(121) Andre, J.-J.; Holczer, K.; Petit, P.; Riou, M.-T.; Clariss, C.; Even, R.; Fourmigue, M.; Simon, J. *Chem. Phys. Lett*. **1985**, *115*, 463.

(122) Turek, P.; Petit, P.; Andore, J. J.; Simon, J.; Even, R.; Boudjema, B.; Guillaud, G.; Maitrot, M. *J. Am. Chem. Soc*. **1987**, *109*, 5119.
(123) Maitrot, M.; Guillaud, G.; Boudjema, B.; Andre, J. J.; Strzelecka, H.; Simon, J.; Even, R. *Chem. Phys. Lett*. **1987**, *133*, 59.
(124) Fujita, A.; Hasegawa, H.; Naito, T.; Inabe, T. *J. Porphyrins Phthalocyanines* **1999**, *3*, 720.
(125) Morimoto, K.; Inabe, T. *Mol. Cryst. Liq. Cryst*. **1996**, *284*, 291.
(126) Morimoto, K.; Inabe, T. *J. Mater. Chem*. **1995**, *5*, 1749.
(127) Matsumura, N.; Fujita, A.; Naito, T.; Inabe, T. *J. Mater. Chem*. **2000**, *10*, 2266.
(128) Mossyan-Deneux, M.; Benlian, D.; Lab, M. L.; Pierrot, M.; Sorbier, J. P.; Fournel, A. *Mol. Cryst. Liq. Cryst*. **1985**, *120*, 437.
(129) Mossyan-Deneux, M.; Benlian, D.; Pierrot, M.; Fournel, A. *Inorg. Chem*. **1985**, *24*, 1878.
(130) Moubaraki, B.; Ley, M.; Benlian, D.; Sorbier, J.-P. *Acta Crystallogr*. **1990**, *C46*, 379.
(131) Janczak, J.; Idemori, Y. M. *Inorg. Chem*. **2002**, *41*, 5059.

CR030649X